



Pontificia Universidad Católica del Perú

Escuela de Posgrado

Investigation of the rheological behavior of polyborosiloxane
with magnetically responsive particles

Tesis para obtener el grado académico de Maestro en Ingeniería y Ciencia de
los Materiales que presenta:

Miguel Alberto Vilca Bendezu

Asesor PUCP (PUCP):

Rolf Grieseler

Co-Asesor de la Universidad no PUCP:

Lena Zentner


Lima, 2024

Informe de Similitud

Yo, Rolf Grieseler, docente de la Escuela de Posgrado de la Pontificia Universidad Católica del Perú, asesor de la tesis titulada “**Investigation of the rheological behavior of polyborosiloxane with magnetically responsive particles**”, del autor Miguel Alberto Vilca Bendezu, código PUCP: 20140242, alumno de la Maestría en Ingeniería y Ciencia de los Materiales, dejo constancia de lo siguiente:

- El mencionado documento tiene un índice de puntuación de similitud de 9%. Así lo consigna el reporte de similitud emitido por el software *Turnitin* el 18/01/2024.
- He revisado con detalle dicho reporte y la Tesis o Trabajo de Suficiencia Profesional, y no se advierte indicios de plagio.
- Las citas a otros autores y sus respectivas referencias cumplen con las pautas académicas.

Lima, 18 de enero de 2024.

| | |
|----------------------------|---|
| Grieseler, Rolf | |
| CE: 001660902 | Firma  |
| ORCID: 0000-0001-5307-7755 | |

Acknowledgements

First and foremost, I would like to express my gratitude to God for blessing me with life and placing me in a loving family like mine. With His guidance and support, one can improve and strive towards goodness - of course, with the help of the right people as well.

A very special thanks to my parents without their help it would not have been possible to start this new adventure, to my mom who supports me every time no matter the distance and time zone, and for all their advice.

Thanks to my advisors at TU-Ilmenau: Dr.-Ing. Lukas Merker for all his help in a previous investigation that helped me a lot to get into this kind of investigation work in another language and country, and for all the patience, preoccupation, and quick response for this work. To Dr.-Ing. Erik Gerlach for their support and guidance in this work. To Prof. Dr.-Ing. habil. Lena Zentner for all her support, advice, and patience for the work and also for their openness to receiving me as a thesis student from another country and specialization area. Also, thanks to Jhohan Chávez for guiding me in the city, showing me the university, and being my first advisor who for improvements in their life had to leave the town and even so he was pending to my progress in all aspects during my stay in Ilmenau.

Thanks to Dr. Rolf Grieseler, my advisor from Peru, for his support during my stay in Ilmenau, especially when problems arose, and help giving me advice to calm down and move forward. Also, for their help and advice on the realization of this work and for the time to teach me how to use the SEM and for taking good images with it.

Thanks to the PUCP team of the laboratory "CITE Materiales PUCP" for their help in performing the complementary tests for the characterization of the material.

Thanks to Dr. Julio Acosta for introducing me to the field of materials and for encouraging me to enter for the master's degree.

Finally, thanks to all my Peruvian and foreign friends for the shared experiences that helped me to continue with this work. Especially to John León and Alejandra Guzmán for being my new brothers and thanks to them it was possible to present this work.

Kurzfassung

Durch die Entwicklung der Soft-Robotik wird der Einsatz neuer oder neuartiger Materialien forciert, die den notwendigen Anforderungen und Ansprüchen in diesem Bereich gerecht werden. In diesem Zusammenhang kommt den sogenannten Smart Materials besondere Bedeutung zu. Diese Werkstoffe haben die einzigartige Fähigkeit, ihre Eigenschaften unter dem Einfluss physikalischer Größen zu verändern, z.B. in Abhängigkeit von der Temperatur, äußeren Magnetfeldern und elektrischen Feldern. Ein solches Smart Material, das in der Vergangenheit nur als Spielzeug verwendet wurde, ist Polyborosiloxane, welches umgangssprachlich auch als "Silly Putty" bekannt ist. Dieses besitzt aufgrund seiner nicht-newtonschen Eigenschaften vielfältige Anwendungsgebiete. Um das Verhalten von Polyborosiloxane durch ein äußeres Magnetfeld beeinflussen zu können, wurden in der vorliegenden Arbeit Verbundwerkstoffe mit einer Matrix aus Polyborosiloxane sowie Partikeln aus Carbonyleisenpulver synthetisiert und untersucht. Die genannten Komponenten wurden nach der Synthese des Polyborosiloxanes aus Polydimethylsiloxane und Borsäure von Hand gemischt, wobei der Massenanteil der dem Polymer zugesetzten Partikel von 20% bis 80% in Schritten von 20% variiert wurde. Zunächst wurden eine Reihe rheologischer Untersuchungen durchgeführt, um die entstandenen Proben hinsichtlich ihres Speicher- und Verlustmoduls zu charakterisieren und zu vergleichen. Um das Fließverhalten des Materials im Schwerfeld der Erde durch ein Magnetfeld zu beeinflussen, wurde eine Helmholtz-Spule genutzt, die sich durch ein konstantes und homogenes Magnetfeld in der Mitte der Spulen auszeichnet. Die aus den Experimenten gewonnenen Ergebnisse zeigen die Fähigkeit des Materials, eine gewünschte Form unter Einwirkung eines Magnetfelds länger beizubehalten.

Resumen

El desarrollo de la robótica blanda está impulsando el uso de materiales nuevos o innovadores que cumplan los requisitos y exigencias necesarios en este ámbito. En este contexto, cobran especial importancia los llamados materiales inteligentes. Estos materiales tienen la capacidad única de cambiar sus propiedades bajo la influencia de variables físicas, por ejemplo, en función de la temperatura, los campos magnéticos externos y los campos eléctricos. Uno de estos materiales inteligentes, que en el pasado sólo se utilizaba como juguete, es el poliborosiloxano, también conocido coloquialmente como "silly putty". Debido a sus propiedades no newtonianas, tiene una amplia gama de aplicaciones. Para poder influir en el comportamiento del poliborosiloxano mediante un campo magnético externo, en el presente trabajo se sintetizaron e investigaron compuestos con una matriz de poliborosiloxano y partículas de polvo de hierro carbonílico. Los componentes mencionados se mezclaron a mano tras sintetizar el poliborosiloxano a partir de polidimetilsiloxano y ácido bórico, variando la fracción másica de partículas añadidas al polímero del 20% al 80% en incrementos de 20%. En primer lugar, se llevaron a cabo una serie de pruebas reológicas para caracterizar y comparar las muestras resultantes en términos de su módulo de almacenamiento y pérdida. Se utilizó una bobina de Helmholtz, que se caracteriza por un campo magnético constante y homogéneo en medio de las bobinas, para influir en el comportamiento de flujo del material en el campo gravitatorio terrestre mediante un campo magnético. Los resultados obtenidos en los experimentos muestran la capacidad del material para mantener la forma deseada durante más tiempo bajo la influencia de un campo magnético.

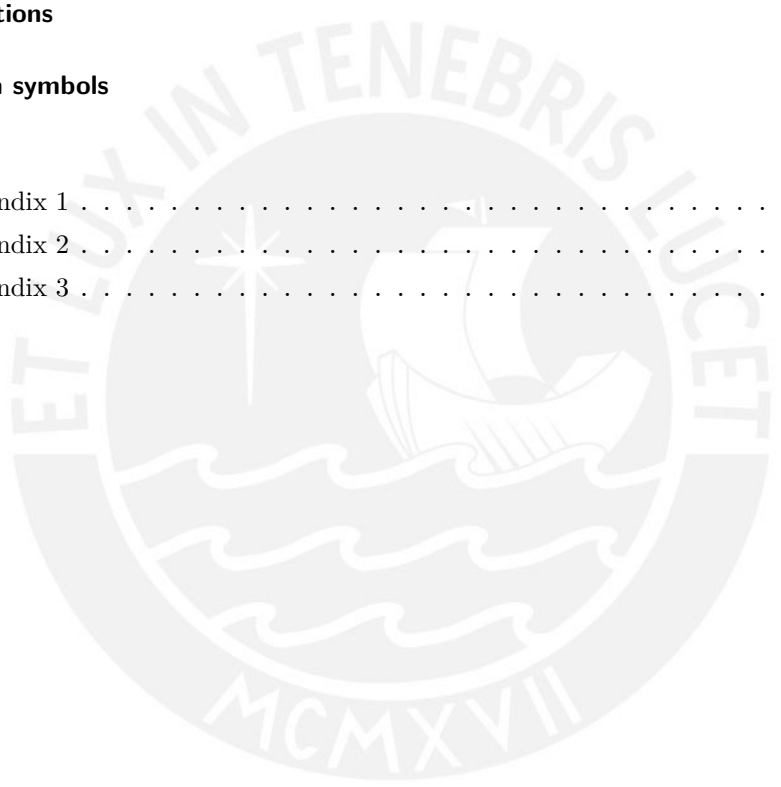
Abstract

The development of soft robotics is driving the use of new or innovative materials that meet the necessary requirements and demands in this area. In this context, so-called smart materials are of particular importance. These materials have the unique ability to change their properties under the influence of physical variables, e.g., depending on temperature, external magnetic fields, and electric fields. One such smart material, which was only used as a toy in the past, is polyborosiloxane, also known colloquially as "silly putty". Due to its non-Newtonian properties, it has a wide range of applications. In order to be able to influence the behavior of polyborosiloxane by an external magnetic field, composites with a matrix of polyborosiloxane and particles of carbonyl iron powder were synthesized and investigated in the present work. The above components were mixed by hand after synthesizing the polyborosiloxane from polydimethylsiloxane and boric acid, varying the mass fraction of particles added to the polymer from 20% to 80% in steps of 20%. First, a series of rheological tests were carried out to characterize and compare the resulting samples in terms of their storage and loss modulus. A Helmholtz coil, which is characterized by a constant and homogeneous magnetic field in the middle of the coils, was used to influence the flow behavior of the material in the Earth's gravitational field by means of a magnetic field. The results obtained from the experiments show the ability of the material to maintain a desired shape for longer under the influence of a magnetic field.

Contents

| | |
|---|------------|
| Acknowledgements | III |
| Kurzfassung | IV |
| Resumen | V |
| Abstract | VI |
| 1 Introduction | 1 |
| 2 State of the art | 4 |
| 2.1 Smart materials | 4 |
| 2.1.1 Magnetorheological fluids | 5 |
| 2.2 Rheological concepts and models | 6 |
| 2.2.1 Rheological basics | 7 |
| 2.2.2 Storage and loss modulus | 8 |
| 2.2.3 Rheological models | 10 |
| 2.3 Polyborosiloxane | 12 |
| 2.4 Carbonyl iron powder | 14 |
| 3 Critical resume and intended goals | 16 |
| 4 Experimental methodology and results | 18 |
| 4.1 Polyborosiloxane synthesis | 18 |
| 4.1.1 Machines and devices | 20 |
| 4.1.2 Materials | 22 |
| 4.1.3 Carbonyl iron powder mixing | 22 |
| 4.2 Rheological characterization | 24 |
| 4.2.1 Amplitude sweep test | 27 |
| 4.2.2 Amplitude sweep results | 27 |
| 4.2.3 Frequency sweep test | 30 |
| 4.2.4 Frequency sweep results | 31 |
| 4.3 Shape change characterization | 34 |
| 4.3.1 Shape change results | 35 |

| | | |
|----------|---|--------------|
| 4.4 | Further characterization | 37 |
| 4.4.1 | Thermogravimetric analysis | 37 |
| 4.4.2 | Fourier transform infrared spectroscopy | 40 |
| 4.4.3 | Scanning Electron Microscope | 42 |
| 5 | Conclusions and future investigations | 48 |
| 5.1 | Conclusions | 48 |
| 5.2 | Future investigations | 49 |
| | Bibliography | IX |
| | Used abbreviations | XV |
| | List of formula symbols | XIX |
| A | Appendix | XX |
| A.1 | Appendix 1 | XX |
| A.2 | Appendix 2 | XXI |
| A.3 | Appendix 3 | XXIV |
| | Statement | XXVII |



1. Introduction

Soft robotics have gained significant attention in recent times. One of the aims of the sub-field is development of materials that improve the interaction between humans and robots. Robotics, on the other hand, is a field that primarily uses hard and stiff materials, hence its nickname, hard robotics. Machines made from rigid structural materials and powered by electrical actuators or pressurized fluids, which can be fixed to the floor or in the form of mobile entities, fall under this category [1]. Hard robotics is commonly used for accurate and precise moves and interactions with the environment. However, one major disadvantage of hard robotics is that they pose a safety hazard to humans [1, 2]. Some of these hazards are related to damage like crushing, scratches, burnings, dislocations, and others to the user or personnel around the environment of the robot. According to the Occupational Safety and Health Administration (OSHA) of the United States, the possible dangers of working with robots are impact, collision, crushing, trapping hazards, being struck by projectiles, electrical, hydraulic, and pneumatic hazards, slipping, tripping, and falling hazards. Worth noting that these hazards occur in most cases during the assembly, maintenance, testing, or installation of the robot. Therefore, the interaction between humans and robots needs to be monitored and controlled at all times for safety reasons [3].

Although hard robotics are quite advanced and are in continuous improvement, soft robotics got a lot of advantages that are guided around its main objective. Create a robot with the capability to adapt immediately to an unpredictable environment, reduce the hazards of interaction with the robot, decrease as much as possible the monitoring of human-robot interaction, increase the amount and kind of tasks made by the robot, etc. [1, 2, 4]. Other advantages of using soft materials are the possibility to move in confined spaces, increased impact resistance, and complex models within the design [2].

Most common soft materials used at time are elastomers, polymer composites, fluids, gels and liquid metal embedded elastomers [2]. As is noted, all the categories are lightweight materials and in some cases, they try to add two or more different properties to take advantage of distinct materials to improve the performance of the final product. The topic of composite materials is an interesting area where there are a lot of combination possibilities to create a lightweight, resistant material that could bear the corresponding mechanical stresses and adapt to the environment through an active or passive stimulus like temperature, magnetic field, electric field, etc. Nevertheless, this wide range of choices could be expanded, and the introduction of a novel smart material is a useful contribution to the scientific community. Thus, the present investigation will help to bring us closer to one of the goals of soft robotics, which is to design robots with new features that permit morphological adaptive changes within unpredictable

environments, such as factories, where changes in parameters may occur due to failures or human error. In which the aim is to reduce damage to personnel or machinery around due to the robot's adaptation to an unexpected situation, in which it will continue to function but will not be a major problem. [4]

The spotlight material in this investigation is polyborosiloxane (PBS). By definition borosiloxanes are individual compounds containing Si–O–B bonds. Under this definition, the compounds are derivative from the reaction of boric-acid (BA) and an organosilicon framing. Thus, a polyborosiloxane is an oligomeric or polymeric structure of a wide number of compounds bonded due to the reaction of their functional groups in their ends. [5]. That have changed through the years improving the material. Some ways to obtain PBS are polycondensation reactions, boron termination reaction, simultaneous polymerization of polydimethylsiloxane (PDMS) with boron ends, etc. [6]. Figure 1.1. shows the two main precursors used for the production of PBS, BA on the left and hydroxy terminated PDMS on the right. These precursors are the used to produce PBS through a polycondensation reaction. Worth noting that these both precursors are not unique, however, they are used due to their availability and the simple synthesis procedure involved in using them.

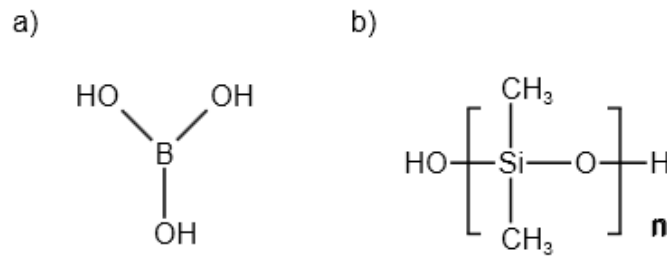


Figure 1.1.: Molecular structure of main precursors of PBS: (a) Boric acid; (b) Polydimethylsiloxane

PBS by itself acts like a non-Newtonian fluid due to its viscous liquid behavior at low deformation rates and rubbery behavior at high rates [6]. However, PBS has the ability to change its final rheological properties by modifying the molecular weight of the PDMS used as precursor. This phenomenon occurs due the formation of hydrogen bonds between Si–O–B(OH)₂ end groups and Si–O:B weak bonding, another cause are the topological entanglements of the molecular chains. This peculiar behavior suggests a simple way to tailor the rheological properties of PBS through the molecular weight of PDMS due to the length of the polymeric chains and the content of boron atoms added to the PBS. [6, 7]

Despite presenting promising properties, PBS has a common difficulty: finding a way to handle and remain it in a desired shape. This problem is related to the non-Newtonian characteristics. That is why usually PBS is used with another material, bonded, mixed, encapsulated or layered like in the last investigations regarding PBS [8–13]. In light of this way to solve the problem of PBS, it is proposed to make a composite material with a matrix of PBS and a reinforcement

of magnetically response particles in order to obtain a smart material capable of changing their rheological and mechanical properties as convenient. A well-known type of particles used in investigations for magneto-rheological fluids and shear stiffening gels, both kinds of materials are pretty similar to the desired composite material to achieve in this investigation, is carbonyl-iron-powder (CIP) [14]. The use of this type of particles proves that they are reliable for this purpose due to their properties described by their manufacturer and proven by different researches [14–19].

The viscoelastic behavior of the PBS can be modeled with physical elements such as dampers and springs. It's also considered a smart material because it has a different behavior depending on the speed of the applied mechanical load. At low strain rates, it can behave as a viscous material, while at high strain rates, it behaves as an elastic material. Adding CIP particles makes it easier to control its properties by controlling the stimulus that triggers the change. The aim of this thesis is therefore to investigate the influence of the mass content of CIP particles in a PBS matrix on the rheological and physical properties of the composite material. From the analysis of its rheological and physical properties. From the analysis of its rheological and physical properties. This will allow future research to have information to use the material in future simulations so that it can be used in complex systems. In addition, it is desired to test if it is possible to obtain a functional material by mixing both elements after the synthesis of PBS. It is important to understand why PBS is considered a smart material, how rheology helps us to study its behavior, and what the literature says about the molecular structure of PBS that gives it these properties. The upcoming chapter will delve into these concepts in detail to gain a better understanding of the reasons behind this peculiar behavior.

2. State of the art

This chapter presents some basic concepts related to the present investigation and a basic introduction to rheological models that will be useful for future research focused on simulation. Also, some peculiar characteristics of the primary materials of the thesis are described.

2.1. Smart materials

Smart materials are a new kind of material that has emerged due to the constant need for advancements and technological improvements. With the ever-increasing demand for materials that meet unique and challenging requirements, smart materials have become popular. Within this thesis, smart materials are defined as those capable of changing one or more properties in response to an input stimulus, which can be present in various physical and chemical phenomena, such as pressure, electric fields, temperature, magnetic fields, chemical reactions, nuclear radiation, and more. That definition can be summarized in advanced materials that react to their environment in a smart way to fulfill, in a better way, their function. [20, 21]

Within smart materials, there are two types of categories to separate them according to the way they react to stimuli. One is called passive; this kind is able to transfer some types of energy. This means that they could transfer energy because they lack the capability to transform the input stimuli. These kinds of materials usually function as sensors. The other one is called active smart materials. This kind, unlike the other, has the ability to do one or two of the next briefly described phenomena. The first transforms the input stimuli (energy) into another kind of energy like piezoelectric materials. The second change their characteristics, properties, or geometry under stimuli. It is worth noticing, that all the smart materials have the capability to return to the initial state of the material once the stimuli have been withdrawn. This means that the changes in the characteristics and properties could return to their original values. [20, 21]. Figure 2.1. shows some examples of a) a passive smart material and b) an active smart material. The passive smart material, in this case, is an optical fiber that allows the transmission of the light that will be read as information in the form of 1 and 0 by a detector. [22]. The active smart material presented is a piezoelectric material. This has the capability to elastic deform when an electric field is applied due to the polarization of the inner crystal structure of the material. The effect also could happen in the inverse situation, a mechanical deformation in the material can polarize it and generate a little potential difference. [23]

Since there are many kinds of stimuli, smart materials are classified into different types according to their stimuli. There are shape memory alloys, piezoelectric materials, magnetostric-

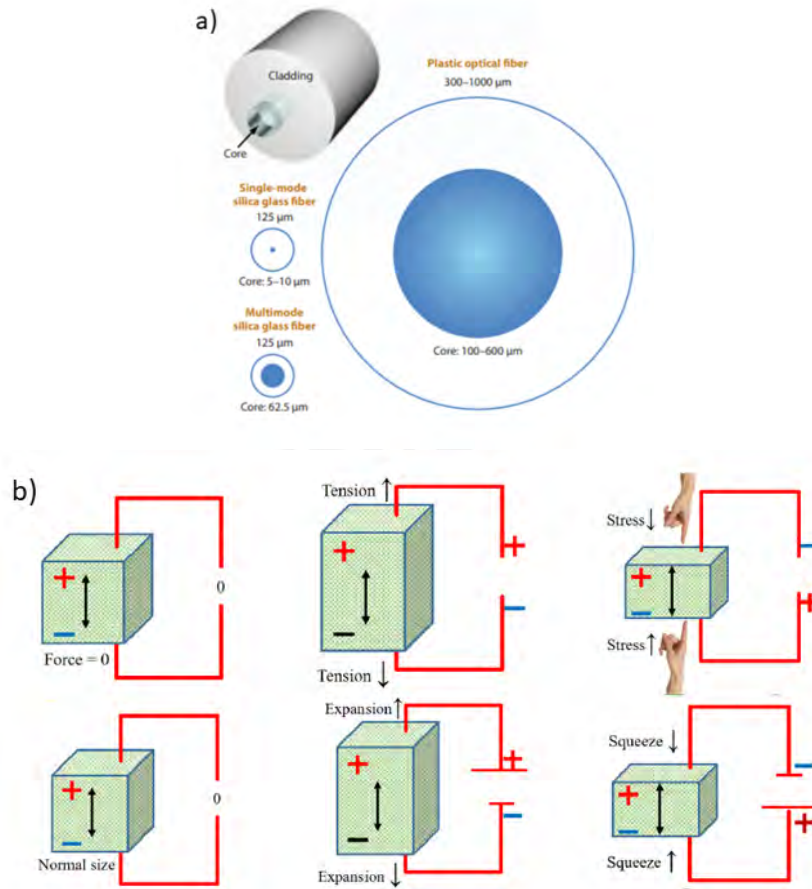


Figure 2.1.: Examples of the different categories of smart materials: (a) Passive smart material (optical fiber); (b) Active smart material (piezoelectric material) [21, 24]

tive materials, electrostrictive materials, chromic materials, pH sensitive materials, electro-rheological fluids, and magnetorheological fluid (MRF) [21]. This thesis focuses on the last type of smart materials, which are briefly discussed in the next paragraph.

2.1.1. Magnetorheological fluids

Magnetorheological fluids are a particular class of smart materials, usually made out of non-Newtonian fluids (non-magnetizable) with suspended micron-sized particles (highly magnetizable). They react when a magnetic field is applied to the material. When the stimuli reach the MRF, the material immediately turns into a nearly solid state [25]. A well-known type of particles used in this field are CIP due to their high saturation magnetization (2.1 T) and low magnetic coercivity. Magnetic materials that possess low coercivity are commonly referred to as magnetically soft materials. This characteristic makes the material behave like a magnet

but momentary, that behavior helps the material to magnetize and demagnetize easily. All these described factors allow for a reversible transformation of MRF. [25, 26]

The most commonly used continuous media are mineral oils, polyesters, polyethers, water, and silicone oils. A common problem with MRFs is that, over time, the suspended particles settle and agglomerate, diminishing the magnetorheological effect. Therefore, it is common to use additives to avoid the sedimentation and aggregation of the particles. Figure 2.2. shows how the suspended particles behave on an MRF a) under normal conditions ($H=0$) and b) under the effect of a magnetic field ($H>0$). It is observed that in normal conditions the particles are randomly distributed among the MRF. Instead, when the magnetic field is applied, the particles align with the direction of the magnetic field. This reorganization leads to an increase in the thickness in the same direction. Also, the viscosity increases and viscoelasticity is induced. [21, 25]

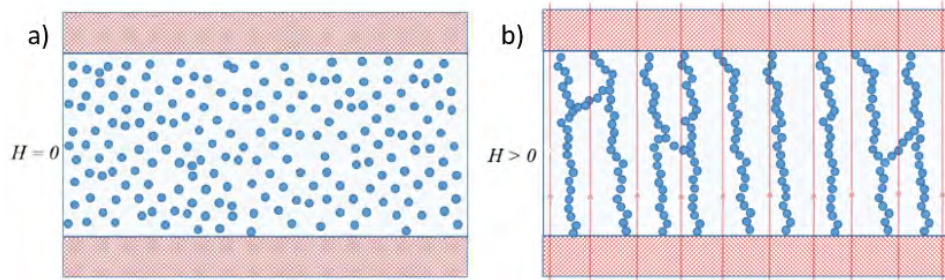


Figure 2.2.: Behavior of MRF: (a) Under normal conditions; (b) Under the effect of a magnetic field [21]

Lately the new tendency is to combine materials in the continuous media like the investigation of Ding et al. They made a mixture of silicone rubber and polyurethane with the particularity that the cross-linking was low, which caused it to behave like a gel. The suspended particles used in that investigation are also CIP. This new blend reach improvements on the shear stiffening effect. The effect is increased 150 times compared to the material made with silicone rubber. This kind of investigation brings notions that the new path for this field is improving the continuous media through different materials. [16]

2.2. Rheological concepts and models

Within the branch of rheology are a wide variety of models to describe the behavior of materials in general. In this section, some of the basic models will be explained to describe the three primary behaviors. These behaviors are

- The completely elastic behavior, where all the energy is stored in the material;
- The completely viscous behavior, where all the energy is dissipated in the form of heat;

- The viscoelastic behavior, which is a mixture of the first two behaviors and depends on the force, time, and deformation.

Some models more suitable for describing the complex behavior of PBS will also be shown. However, it is essential to understand the fundamentals of rheology in order to properly understand the subsequent models. [27]

2.2.1. Rheological basics

There is an idealized situation to explain the rheological phenomenon that is called two plates model. The lower plate remains stationary, and the upper plate tries to move due to an applied force F . Between both plates is the fluid desired to measure, and the height of the gap is labeled h . The force causes a displacement Δx of the upper plate, deforming the fluid on the initial space and taking the shape of the red discontinued lines shown in Figure 2.3. The area A of the fluid in contact with the upper plate is under a shear stress σ defined in Equation 2.1. [27]

$$\sigma = \frac{F}{A} \quad (2.1)$$

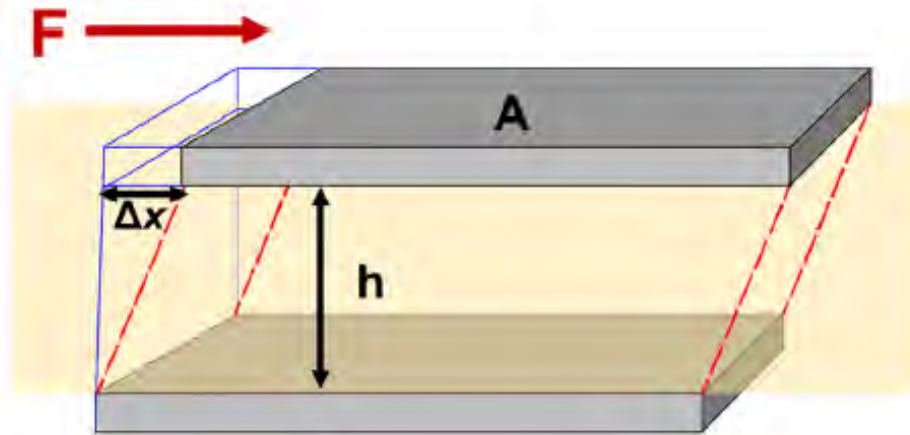


Figure 2.3.: Two plate model[27]

Figure 2.3. shows that the displacement is not constant along the gap. This is due to the immobility of the lower plate, which creates a fluid velocity gradient along the gap, where the fluid surrounding the lower plate tends to try to maintain its position and the fluid zone closer to the upper plate will try to follow the velocity of the upper plate. The gradient also affects the shear strain γ , which can be calculated by Equation 2.2. [27]

$$\gamma = \frac{\Delta x}{h} \quad (2.2)$$

A peculiar behavior in fluids is that the shear strain will increase along the time the stress is applied. This change in the speed is called shear rate $\dot{\gamma}$ that is represented in Equation 2.3. [27]

$$\dot{\gamma} = \frac{\Delta\gamma}{\Delta t} \quad (2.3)$$

The shear or also called dynamic viscosity η (Equation 2.4) represents the relation between shear stress and shear rate. [28]

$$\eta = \frac{\sigma}{\dot{\gamma}} \quad (2.4)$$

There are many kinds of fluids classified by their flow behavior. Like Newtonian fluids that obey Newton's law of viscosity, which means that the viscous stress is proportional to the velocity gradient. They also present a viscosity not related to the shear rate [28]. In contrast, fluids that do not follow Newton's law are called non-Newtonian fluids. These are classified into shear thickening and shear thinning. Shear thickening is a phenomenon in fluids that increase their viscosity when the shear rate or shear stress increase. This kind of fluids are also called dilatant materials [27]. Instead, shear thinning is when a fluid decrease its viscosity when the shear rate increase. They are also called pseudoplastics due most of the polymers when they are in a like fluid state shows these characteristics. [27, 28]. Figure 2.4. shows, a summary of types of fluids and their behavior when a) shear stress is present as function of shear rate and b) viscosity as function of shear rate. [28]

2.2.2. Storage and loss modulus

Both parameters, storage modulus G' and loss modulus G'' , are essential to comprehend the behavior of fluids. G' represents the real part and G'' represents the imaginary part of the complex dynamic modulus G^* . [29]. Equation 2.5 shows how the relation between G' and G'' can be represented by the tangent of the phase angle δ . The Figure 2.5. illustrates the components of the complex dynamic modulus on the real and imaginary axis, and their correlation with the phase angle. [27, 30]

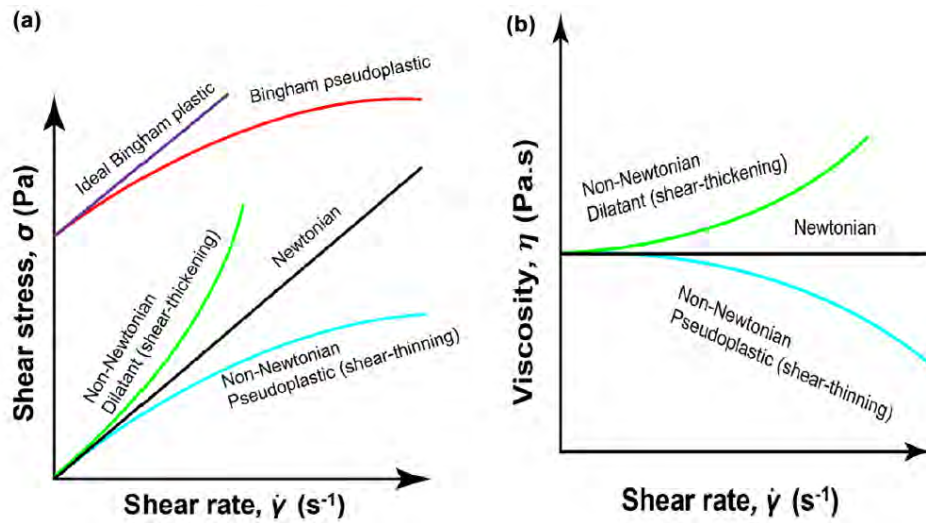


Figure 2.4.: Summary of different types of fluids: (a) Shear stress as function of shear rate; (b) Viscosity as function of shear rate. [27]

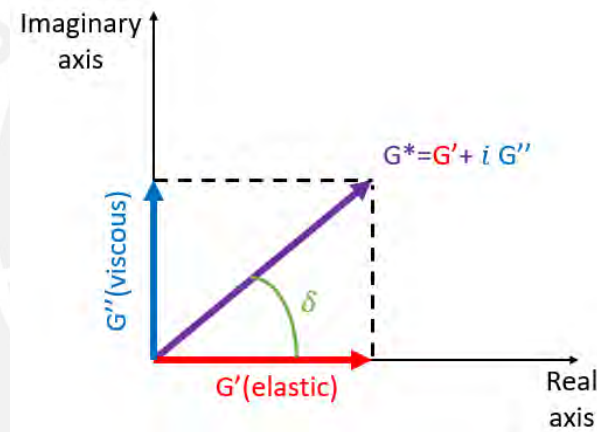


Figure 2.5.: Complex dynamic modulus adapted from [30]

$$\tan \delta = \frac{G''}{G'} \quad (2.5)$$

Regarding the meanings and representations, the storage modulus is the energy that material is capable of, as the name says, to store and is possible to release when an external force stops applying. By contrast, the loss modulus is the energy that is dissipated in another form of energy, usually as heat. Both representations are shown in Figure 2.6. by the example of a bouncing ball made of a viscoelastic material. [27, 30]

The phase angle will be further used to understand the working principle of the rheometer.

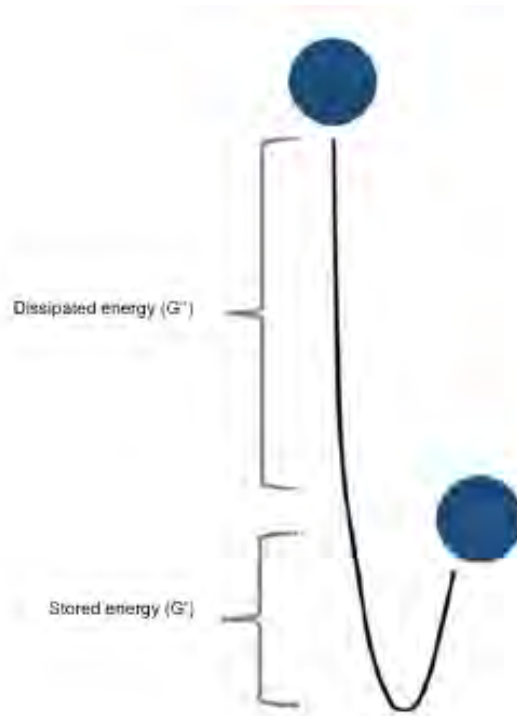


Figure 2.6.: Example of storage and loss modulus, extracted from [27]

2.2.3. Rheological models

First, the elastic behavior is presented. In this case, the material is in its minimum equilibrium state at rest. When a deformation or force is applied, the equilibrium is lost, and the material tries to return to its original state due to an elastic force. This behavior is modeled as a spring where the shear strain is defined as in Equation 2.6 following the Hooke's law. [27, 30]

$$\gamma = \frac{\sigma}{|G^*|} \quad (2.6)$$

A second model describes the purely viscous behavior. Here the material can be represented by a damper. When stress is applied, the material starts to deform at a constant rate until the stress stops. Then, the energy used to obtain the displacement or deformation is dissipated by the material in form of heat increasing the inner temperature. Equation 2.7 shows the shear strain for this model. It can be observed, that this process is time dependent. [30]

$$\gamma = \frac{\sigma \cdot t}{\eta} \quad (2.7)$$

One issue with the models is that the springs are not designed to handle shear stresses. Therefore, it is not appropriate to use a spring and relate it with shear modulus G and shear strain γ . Instead, the modulus of elasticity E and engineering strain ϵ are more suitable for this purpose. However, it is possible to relate the modulus of elasticity to the shear modulus with the following approximation, as shown in Equation 2.8, a formula obtained from Hooke's law generalized with isotropic materials. [27]

$$G = \frac{E}{2 \cdot (1 + \nu)} \quad (2.8)$$

Although the approximation is well-suited, it has certain conditions. It is assumed that the material possesses isotropic properties and a Poisson ratio ν of 0.5. This condition must be met because the expression works just for isotropic materials. A Poisson's ratio of 0.5 is used because the rheology deals with fluids and materials with this Poisson's ratio value are characterized by being isotropic and incompressible, just like fluids. All these considerations are taken into account to make a tensile test on springs possible and to obtain the tensile elastic constants, which are easier to obtain than the shear constants. [27]

The third model describes a unique behavior called viscoelasticity, which is a combination of both the aforementioned behaviors. Many models have been proposed over the years to explain this peculiar behavior. Here, three viscoelastic models will be described. The first viscoelastic model is called the Maxwell model, which consists of a spring and damper arranged in series. The predominant behavior is highly dependent on the duration of the applied stress. At short application times, the elastic behavior dominates, while at long application times, the viscous behavior governs. Equation 2.9 shows the shear strain for this model. [27, 30]

$$\gamma = \sigma \left(\frac{1}{G} + \frac{\sigma t}{\eta} \right) \quad (2.9)$$

The second viscoelastic model is called the Voigt-Kelvin model. In this case, the spring and damper are arranged in a parallel connection. Shear deformation takes time to develop because the damper delays the response of the spring. This delay causes the material to mimic a viscous fluid at short times, then behaves like an elastic material due to the limited deformation of the spring. Due to the transition a new parameter called relaxation time τ is introduced and is shown in Equation 2.10. This parameter is the time required to reach 63% of the shear deformation of its asymptotic. [27, 30]

$$\tau = \frac{\eta}{G} \quad (2.10)$$

With relaxation time defined it is possible to calculate the shear strain for the Voigt-Kelvin model as Equation 2.11 shows.

$$\gamma = \frac{\sigma}{G} \cdot \left(1 - e^{-\frac{t}{\tau}}\right) \quad (2.11)$$

The Burgers model is considered the most precise model to describe viscoelastic materials. This model consists of two other well-known models, the Maxwell, and Voigt-Kelvin models, connected in series. The spring, Voigt-Kelvin model and damper are arranged in this order. In Figure 2.7., shows the 4-element model on the left and the behavior of shear strain over time on the right. As per Equation 2.12, the approximation of shear strain includes three components that represent elastic, viscoelastic, and viscous contributions, respectively from left to right. This model is a great approach to studying viscoelastic behavior and can help obtain the required parameters. One of its advantages is that it is related to the creep test. [27, 30]

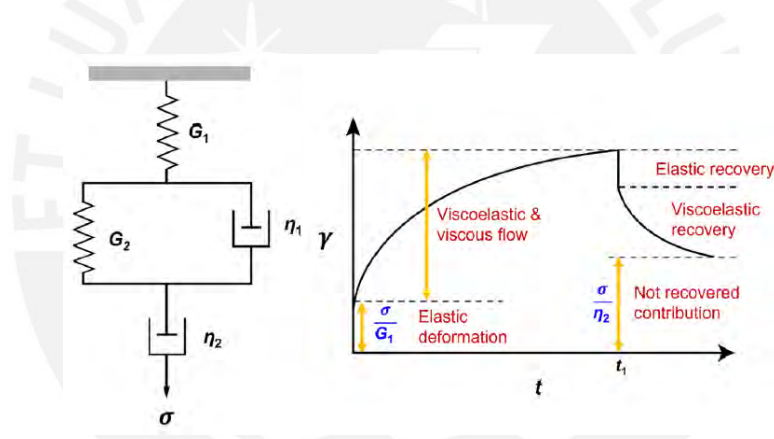


Figure 2.7.: Burgers or four element model and its shear strain response through time [27]

$$\gamma = \sigma \left(\frac{1}{G_1} + \frac{1}{G_2} \cdot \left(1 - e^{-\frac{t}{\tau}}\right) + \frac{t}{\eta_2} \right) \quad (2.12)$$

The creep test involves applying a constant stress to a material for an extended period at a high temperature to study its low and steady flow. It is important to note that this test must be carried out within the linear viscoelastic region (LVER). [27, 30]

2.3. Polyborosiloxane

As mentioned in the introduction, PBSs are compounds characterized by containing Si–O–B bonds with a high molecular weight due to their oligomeric or polymeric structure [5]. Figure

2.8. displays the chemical structure of PBS. The reaction with the BA has three possible final structures due to varying PDMS chain lengths. The structures are

- Structure I results from a direct poly-condensation of PDMS and BA;
- Structure II has B–O–B bonds on its sides due to an additional polymerization that occurs among BA;
- Structure III results from two more polymerization reactions of BA, producing a cyclic PBS. [6, 31]

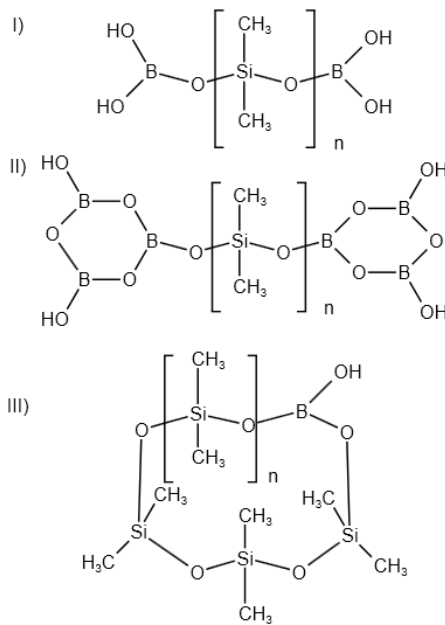


Figure 2.8.: PBS possible molecular structures, proposed by Zinchenko et al. [6, 8, 31]

As noted, BA could react with its molecules by an additional polymerization process. However, the amount of additional polymerization reactions depends on the synthesis methodology. When using an extra BA content and a polycondensation reaction, the PDMS will react only with the necessary BA; the remains of the latter precursor will not react and can be visualized. [6, 32]

Regarding properties, PBS has a highly flexible siloxane backbone inherited from its precursor, PDMS [5]. In addition, the peculiar viscoelastic and non-Newtonian properties are acquired by the temporary Si–O:B crosslinking between chains. This bond is constantly made and broken due to the interaction of the chains in areas where boron has vacant orbitals available to interact with the unshared electron pairs of the oxygen atoms of the other chains. Figure 2.9. shows the representation of the interaction between chains due to the boron and oxygen content. An additional peculiarity of this physical crosslinking is that it allows the material to

act as a self-healing material; both parts must be brought together to rejoin without difficulty. [5, 6]

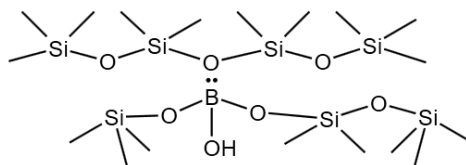


Figure 2.9.: Temporary cross-linking bonds between chains, adapted from [33]

The working mode of physical cross-linking depends on the applied strain's speed. Figure 2.10. shows the four different behaviors that have PBS according to strain rate. First is the equilibrium state, where only gravity affects the material and allows the Si–O:B bonds to join and break. When a low strain rate is applied, it acquires a viscous state, and the chains have time to disentangle and some Si–O:B bonds to break. [34]

Nevertheless, if the strain rate increases, the Si–O:B bonds break and dynamically reform so quickly that they prevent disentanglement. This condition is reflected in the rubbery state of the material, giving it the property to absorb the energy of the impact, leading to an elastic-like material. Finally, when the strain rate reached a critical value, PBS transitioned to a glassy state. PBS drastically increases its stiffness in this condition and behaves like a brittle material, breaking the siloxane backbone. [34]

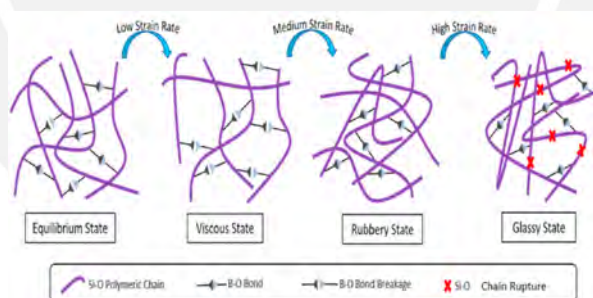


Figure 2.10.: PBS speed dependent behavior, extracted from [34]

2.4. Carbonyl iron powder

Carbonyl iron powder is a well-known type of magnetically responsive particle used in many MRF, shear stiffening gel (SSG), and viscoelastic materials investigations. It is so named because of the raw material for its production, iron pentacarbonyl $\text{Fe}(\text{CO})_5$. [35]. The obtaining process is the following one:

1. Thermal decomposition of iron pentacarbonyl above its boiling point;

2. Radiating growth of CIP particles from a nucleus (onion structure);
3. Chemical vapor decomposition allows the spherical form.

Due to its highly studied process, there are several types. Within these types, CC is a matter of interest. The chemical composition is shown in Table 2.1. This type is considered a soft grade, meaning that the particles undergo an extra process of annealing under a hydrogen atmosphere to reduce nitrogen, carbon, and oxygen. [36]. This type is widely used for its ease of magnetization and demagnetization due to its low magnetic coercivity and high magnetic saturation. [17, 19, 25]

Table 2.1.: Chemical composition and average diameter of CIP type CC [36]

| Chemical composition and average diameter | | | | | |
|---|-------------|------------|------------|------------|------------------------------------|
| Type | Fe min. (%) | C max. (%) | N max. (%) | O max. (%) | Average diameter (μm) |
| CIP CC | 99.5 | 0.05 | 0.01 | 0.18-0.35 | 3.8-5.3 |



3. Critical resume and intended goals

According to the reviewed studies, the molecular weight of the PDMS precursor can determine PBS's final properties. Thus, it is possible to obtain PBS with different properties. The methodology of Reuß has been chosen among various synthesis methods because it was used by the same research group (Mechanik Nachgiebiger Systeme) as this work. This process is followed to enable the production of a consistent and standard type of PBS using fixed precursors. The specific process is detailed below in Section 4.1.

Although some papers have discussed the use of materials that bind PBS with CIP particles, they have yet to give much attention to how the particle content affects the rheological and physical properties of the composite material. Additionally, they have yet to examine whether this material can maintain its shape over time when exposed to a magnetic field.

This work aims to study how the particle content of CIP in a PBS matrix affects the final properties of the composite material. In addition, the analysis will determine whether a functional material can be obtained by mixing CIP with PBS after PBS synthesis. If this mixing condition is satisfactory, the material will be produced in the desired ratio with the prefabricated materials. This process will reduce the time required to obtain the material since the laborious synthesis process has already been completed. In addition, the composite material is expected to maintain dimensional stability when subjected to a magnetic field. It should exhibit minimal or no variations, regardless of whether the field is constant or pulsed.

In order to analyze this peculiar composite material properly, it is recommended to observe its behavior under an external stimulus, such as a magnetic field. When subjected to a magnetic field, a photographic analysis is taken every 10 minutes to study the material's ability to maintain its desired shape over time. The rheological behavior is studied by conducting amplitude and frequency sweep tests. An interface analysis is also done through SEM to study the interaction between the matrix and the reinforcement. FTIR and TGA are also performed to determine if there are any interactions between PBS and CIP or if they coexist in the same space.

The tasks to achieve the main objective of the work are the following:

- Manufacturing different kinds of composite material based on changing the weight content of magnetically responsive particles;
- Investigation of the rheological behavior of the composite materials;
- Investigations of the capability to maintain a desired shape of the composite materials;
- Characterization tests of the composite materials;

3. Critical resume and intended goals

- Conclusions of the obtained results through experimental methodology;
- Recommendations and further investigations.



4. Experimental methodology and results

This chapter provides a detailed explanation of the processes involved in manufacturing PBS and composite material. In addition, it covers the standardized tests used to characterize the composite material and some non-standardized tests that help analyze the material's ability to maintain a desired shape over time, quantitatively and qualitatively.

4.1. Polyborosiloxane synthesis

There are several ways to synthesize PBS, all of which have different advantages and characteristics. All have similar steps, but the aim is the same: form hydroxyl groups in a siloxane chain to allow the reaction with the BA. In this section, some of them will be described.

Fan et al. heat BA to 160 °C for 2 hours to obtain pyroboric acid $H_2B_4O_7$, a product of dehydration or polymerization of BA. Then, it is mixed with dimethyl silicone oil. Alcohol is added to improve the dispersion of pyroboric acid. Finally, the mixture is heated in an oven at 250 °C for 8 hours.[17]

Seetapan et al. mix BA with hydroxy-terminated PDMS heated at 120 °C for 48 hours. In this process, the molecular weight of the PDMS has an essential influence on the final properties, such as elastic modulus. Furthermore, the mix ratio between precursors has a strong influence, too. [37]

In this investigation, a procedure similar to that of Seetapan et al. was followed to produce PBS. This decision was taken per a proposal by the department where this investigation took place at TU Ilmenau, Mechanik Nachgiebiger Systeme, in English Department of Compliant Systems. Investigations regarding PBS and prior investigators have created the research bases to continue. In addition, a brief prior investigation of two kinds of PBS, their production, rheological characterization, and properties demonstration through a tensegrity-like structure was made in collaboration with Ramirez and Weber. In that previous investigation, the synthesis steps were established, following the steps described by Reuß to establish a kind of PBS for further investigations and improvements. In this investigation, those aforementioned steps were followed to continue investigating that kind of PBS. [38]

The first step is determining the appropriate hydroxy-terminated PDMS based on the desired final characteristics founded on viscosity. This statement means that PDMS of high viscosity can be chosen to obtain PBS with high ductility or low viscosity to obtain PBS characterized by brittleness. After setting the amount of material to be produced, 40 g of PBS per batch, both precursors are mixed. It should be noted that the amount of BA is 3% (1.2 g) of PDMS's

weight, as Reuß recommended, and the mass of PDMS is the same as the wanted to produce of PBS. This amount of mass of PDMS is used to compensate for material losses due to synthesis. [32, 39]. The amount of BA is above that required to react; however, it is used in excess to ensure a complete reaction of the hydroxy-terminated PDMS and to accelerate the reaction, reducing synthesis time and improving the process. Reuß calculated the stoichiometric amount that depended on the molar mass of the PDMS. For this case, having PDMS of viscosity 750 cSt, the stoichiometric amount of boric acid is 1.47% of the mass of PDMS. The remainder will exist as small white particles in the material. [32]

Then, the mixture was submerged in an oil bath over a magnetic heater stirrer. The oil was at 100 °C and can be of any kind. While the oil bath heats the mixture, a magnetic stir bar inside the mixture will start to rotate. A constant rotation speed of 80 rpm was used because this speed allows the precursor to be mixed and is the minimum possible speed of the device. Faster speeds could lead to the spill of the precursors outside the beaker, reducing the efficiency of the reaction. It should be considered that when the mixture beaker is submerged in the oil bath, the oil level must be above the mixture level. This condition ensures homogeneous heating of the entire mixture by having the same heat transfer conditions. When the mixture is submerged, adjust the heat of the magnetic stirrer to maintain the oil temperature at 100 °C. Consider that a mass group entering contact with oil will reduce its temperature.

Leave the mixture for the maximum amount of time, stirring until the mixture becomes very thick and the stirrer cannot move anymore. To consider that the mixture process before and during the bath oil must be done quickly to avoid aggregation of the BA particles. Previous milling of the BA particles is required to obtain particles as small as possible to improve the interaction of both precursors. After the mixture is done, the product is placed in an oven at 130 °C for 18 hours to evaporate the water product of the polycondensation reaction. Consider that the mix will be reacting constantly and that it is desired to eliminate the water acting as an inhibitor. Also, it is recommended to move the material to a recipient with a large area as much as possible before putting it inside the oven to improve the elimination of water inside PBS. After the time in the oven, the material will present some craters on the surface due to the trapped water that was eliminated when passing to steam. Before using the oven, the synthesis process was developed within a laboratory fume cupboard to prevent introducing strange particles, gases, and fumes.

A problem of this synthesis is the adhesion of PBS to the walls of the beaker and the laborious extraction of the material, which results in a percentage of lost material. After some sample synthesis, it could be determined that the waste percentage is approximately 10%. For more detail on the mass losses during the synthesis, see Appendix A.1.

The following section describes the devices, accessories, and materials utilized.

4.1.1. Machines and devices

The devices used for the synthesis process are simple and relatively inexpensive. A precision balance with a 0,001 g resolution is needed to measure the weight with a low error ($\pm 0,01$ g). It is a Kern model KB 360-3N with a maximum weight capacity of 360 g. Consider that two different glass beakers are needed, one to contain the mixture and the other to be filled with oil. It is recommended to use a lower beaker to contain the oil to have space to manipulate the tallest beaker with the mixture.

A stirrer, preferably with a heating function, is needed to mix the materials. The magnetic stirrer used in this investigation is an Ohaus model Guardian 3000. It is described as a hotplate and stirrer with the advantage of reaching high temperatures quickly.

A mortar is used to mill and crush the BA particles to reduce the size and increase the surface area in contact for both materials. Then, to measure the temperature of the oil bath, a digital thermometer with a display will allow access to the measurements more comfortably. The entire setup (Figure 4.1.) is shown below, where the magnetic stirrer is set to maintain the oil bath at 100 °C.

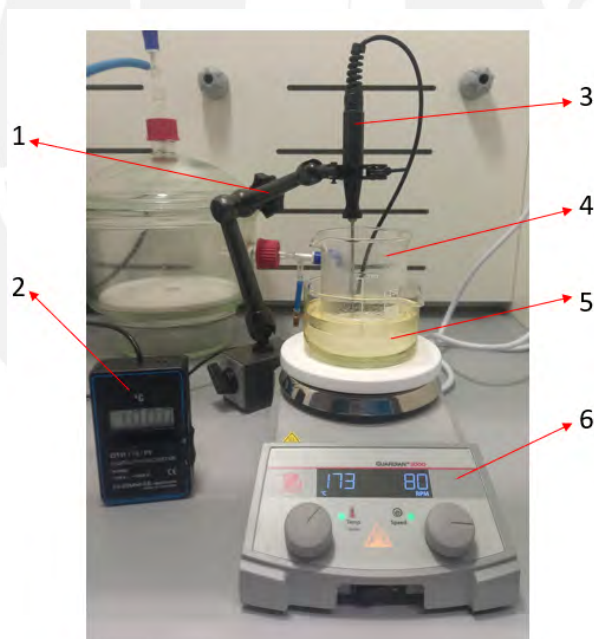


Figure 4.1.: Complete set up for the synthesis of PBS: 1.Universal magnetic stand; 2.Temperature display; 3.Thermometer; 4.Tall beaker (mix go inside); 5.Low beaker (Oil go inside); 6.Hotplate magnetic stirrer

Figure 4.2. shows the oven Binder model FD 23. It has a forced convection system that helps to retire the steam with the help of the adjustable air exhaust. Also, it has a controller with a

timer function that is ideal for setting the heat for the needed time. This model is used to dry and heat samples.



Figure 4.2.: Oven Binder Model FD 23 with timer function and air exhaust

Finally, the fume cupboard (Figure 4.3.) is used for all synthesis processes, inside which the final configuration is arranged. This device protects the user from product fumes and avoids inclusions of foreign particles.



Figure 4.3.: Laboratory fume cupboard Brand Waldner model secuflow: 1.Quick access windows; 2.Inner Plug; 3.Complete set up

4.1.2. Materials

Boric acid is from Sigma-Aldrich and is labeled as B6768-500G with a purity of $\geq 99.5\%$. The particles of this product are pretty big, which must be milled and crushed with a mortar to improve the interaction with PDMS.

Hydroxy terminated PDMS was purchased from the brand Sigma-Aldrich with code 481963-500ML. It has a viscosity of 750 cSt. This viscosity was selected due to previous investigations regarding the influence of the viscosity of PDMS in the final properties of PBS, where the PBS, made with higher viscosity, demonstrated softer properties beneficial for the inclusion of particles inasmuch as the PBS with lower viscosity was stiffer and brittle; poor characteristics to add particles. Although the addition of particles during synthesis is more common, in this research, it is desired to verify that the mixing can be done after synthesis to be able to acquire the composite material when it is needed, having as raw material PBS already synthesized and stored together with CIP that does not require previous preparation. That is why PBS with brittle behavior is not suitable for mixing after it is synthesized because it would break when kneaded or folded. On the other hand, PBS with lower hardness and storage modulus can be folded, kneaded, and stretched without any problem, which allows a simple process of introducing the CIP to the PBS. [38]

Carbonyl iron powder type CC was purchased from Imhoff & Stahl GmbH. Type CC stands out for being used in producing MRFs and SSGs. Its behavior toward magnetic fields is suitable for a magnetization and demagnetization cycle. This characteristic has been proven by the many investigations related to MRF and SSG that have used CIP as a magnetically responsive particle and where satisfactory results have been obtained. [14–19, 25, 26, 40, 41]. Liu et al. investigated the magnetic properties of a composite with CIP and chlorinated polyethylene (CPE). The hysteresis loop with different CIP content ratios is shown in Figure 4.4. extracted from the aforementioned research obtained by a vibrating sample magnetometer (VSM) test. [8]. Their results show a saturation magnetization σ_s of 205 emu/g, where emu stands for electromagnetic unit and represents volume. The coercivity H_c is 20 Oe. As the hysteresis loss is the area between the curves, the CIP loss is shallow due to its small coercivity value. The loops are so narrow that they are seen as a single curve for each specimen in the plot. It can also be noted that the remanent magnetization is of a relatively small value close to zero. For this reason, the CIP can magnetize and demagnetize rapidly. [8]

4.1.3. Carbonyl iron powder mixing

Investigations regarding CIP use different processes to add the particles to the material they are using. Lai et al. mixed the particles with the help of a miniature mixer fitted with a counter-rotating roller impeller where the acrylonitrile butadiene styrene (ABS) pellets and

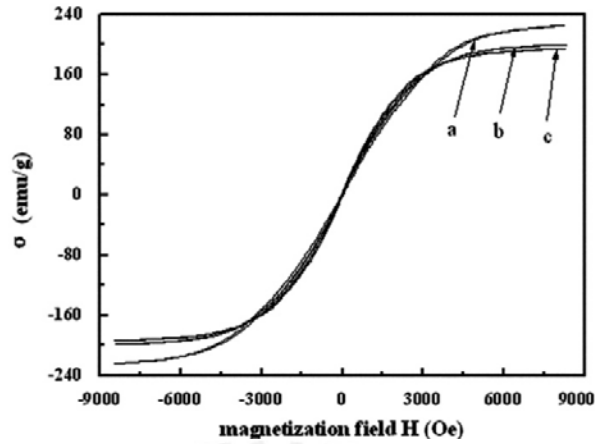


Figure 4.4.: VSM results of CIP ratios of CIP:CPE a.12:1; b.14:1; c.16:1, extracted from [8]

CIP particles were placed. The mixer heats the material around 225 °C for 10 minutes at a rotor speed of 30 rpm. [40]. Zhang et al. introduce the CIP while the polymer matrix is in the polymerization process; this means the particles will spread along the matrix while it solidifies at room temperature. [41]. As is noted, the described processes introduce the particles during the softening of the polymer in the first case or during the polymerization process like in the second case. For this investigation, it was decided to mix the particles after the PBS synthesis. This method is a way to prove the possibility of making the composite material with materials already synthesized or stored. In this case, one research objective is to analyze the influence of the CIP content on the final properties. Five samples were fabricated with different CIP contents, 20%, 40%, 60%, and 80%, where the mass fraction of the particles. The mass of each sample was set at 10 g. Table 4.1. shows the summary of the mass content of the samples and their assigned names.

Table 4.1.: Composition of prepared samples

| Composite material samples | | |
|----------------------------|-----------|-----------|
| Sample | PBS (wt%) | CIP (wt%) |
| PBS | 100 | 0 |
| PBS-20 | 80 | 20 |
| PBS-40 | 60 | 40 |
| PBS-60 | 40 | 60 |
| PBS-80 | 20 | 80 |

As mentioned before, the introduction of the particles in this case is made after the polymerization and obtaining of PBS. Figure 4.5. shows the process of mixing PBS with CIP. It is mandatory to use safety equipment when the CIP is manipulated. This safety measurement is essential because the particle size of CIP is relatively small on the micron scale. Being CIP of this size, it is possible to inhale, ingest, embed, or get into the eyes. It is also suggested that protective measures be used when handling BA synthesizing PBS. These protective measures

are taken to avoid immediate and long-term damage to the person handling these materials. In this case, goggles, masks, gloves, and lab coats were used as protective equipment.

First, the weight of the PBS and CIP is measured to mix the two materials. Afterward, the PBS was spread to create a vast area to facilitate particle insertion. Then, the polymer is folded over the area with surface deposited particles. Subsequently, the polymer is kneaded until the particles are inserted into it. It can be verified by observing the polymer's homogeneous and bright color. If it looks opaque, the particles have not yet entered the polymer. Finally, repeat the process until the material is homogeneous and store it in a labeled storage bag. All mixing processes lasted approximately 1 hour and 40 minutes, and they were done by hand due to the difficulty of handling the particles that could be dispersed in the environment. The particles can fly away when kneading the polymer since they are dry and lightweight. A slight movement of air due to the movement of the polymer can cause loss of particles that fly away and are lost in the environment. This event can also be detrimental to health as it increases the possibility of entering the eyes or being inhaled. For these reasons, it is essential to use the appropriate protective equipment.

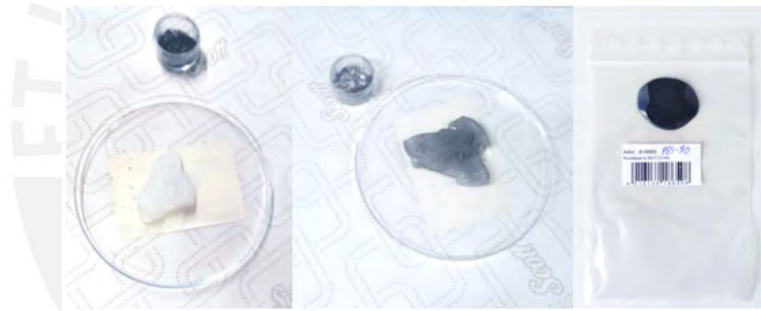


Figure 4.5.: Mixing process of PBS and CIP

4.2. Rheological characterization

The terms storage G' and loss modulus G'' were explained in Subsection 2.2.2. This section will explain how a rheometer works and how it measures both important moduli to understand the material's rheological behavior and their results.

Rheometers are devices designed to measure rheological properties according to the requirements of the material. Therefore, there are many kinds of rheometers, where the rotational rheometer is most used in the field of investigations of MRF and SSG. This kind of rheometer uses the plate-plate model to measure the rheological properties. However, there are two kinds of configuration, Figure 4.6. shows a) plate-plate geometry and b) cone-plate geometry.

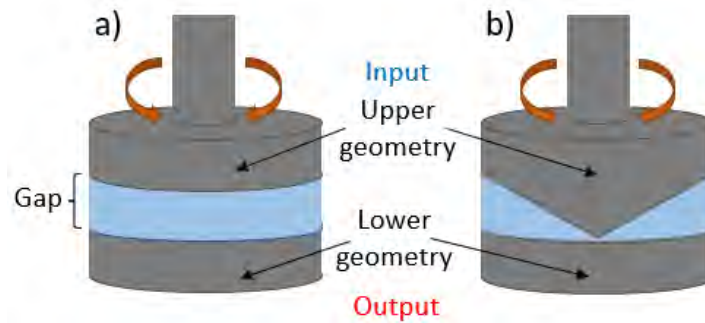


Figure 4.6.: Two types of geometries within rotational rheometers: (a) Plate-plate geometry; (b) Cone-plate geometry, adapted from [30]

Both setups have their specific characteristics. In the first setup, plate-plate geometry, the shear rate increases from the center to the edges of the plates. However, this could be reduced by using small sizes for the gap (space between plates designed to be fulfilled by the material). An advantage of this geometry is that the gap can be highly adjustable and does not have problems with materials with suspended particles. [30, 42]. The second setup, cone-plate geometry, allows the shear rate to be constant along the radial direction due to the cone on the upper geometry. Here, the problem is the small space between the tip of the upper geometry and the surface of the lower geometry. This little space represents a severe problem for materials that have suspended particles owing to the possibility of getting trapped there. Also, the gap height is restricted by the tip of the cone. [30, 42]

Rotational rheometers have an input that can be either torque-controlled or speed-controlled. This means it is possible to apply a torque and measure rotational speed or the other way around, apply a rotational speed and measure torque. Because oscillation tests are used in this case, the upper geometry will go back and forth, resulting in a sinusoidal input signal for the torque or rotational speed. The upper geometry executes the input signal by employing an electronically commutated motor to achieve oscillatory motion. [43]. Figure 4.7. shows the input (blue line) and output (red line), where the input is applied by the upper geometry and the output is sensed by the lower geometry. The three possible behaviors of the material are represented: elastic, viscous, and the combination of both, viscoelastic. The delay between the input and output signals is called phase angle δ and is related to the complex modulus G^* . This angle helps to calculate the real and imaginary part of G^* . Depending on the value of the angle, it is possible to identify the material's behavior. [27, 30]

Since a viscoelastic material is analyzed, it is suitable for performing a dynamic mechanical analysis (DMA). This technique analyzes the viscoelastic behavior through the parameters in Table 4.2. [44]

4. Experimental methodology and results

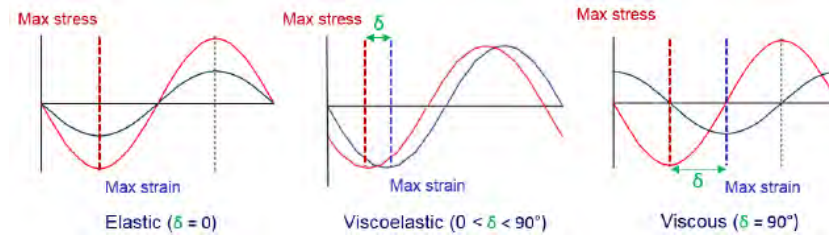


Figure 4.7.: Input and output measures of a rheometer representing the behavior of a elastic, viscoelastic and viscous material, extracted from [30]

Table 4.2.: Viscoelastic parameters possible to measure through DMA

| Result parameters of DMA | | |
|--------------------------|---------------------|----------------|
| Term | Elongation/traction | Rotation/shear |
| Modulus | E | G |
| Complex modulus | E* | G* |
| Storage Modulus | E' | G' |
| Loss modulus | E'' | G'' |
| Loss factor | $\tan(\delta)$ | $\tan(\delta)$ |

Within the DMA, two tests were used in this investigation: the amplitude and frequency sweep test. Both were performed in the same rheometer from Malvern in collaboration with Netzsch model Kinexus Pro +. Figure 4.8. shows the rheometer with its protective hood that allows it to remain at a controlled temperature and avoid introducing strange bodies or spreading the tested material. A refrigerated circulator maintains a temperature of 25 °C in the rheometer inside the protective hood. The latter is a Julabo model CF41.

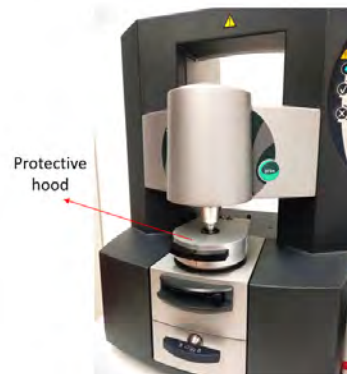


Figure 4.8.: Rheometer Malvern-Netzsch model Kinexus Pro +

Finally, the setup used for both tests is plate-plate due to similar results as the cone-plate for small gaps, as shown in the investigation of Reuß [32]. Both plates have the same dimension of $\varnothing 25$ mm. Figure 4.9. shows both geometries.

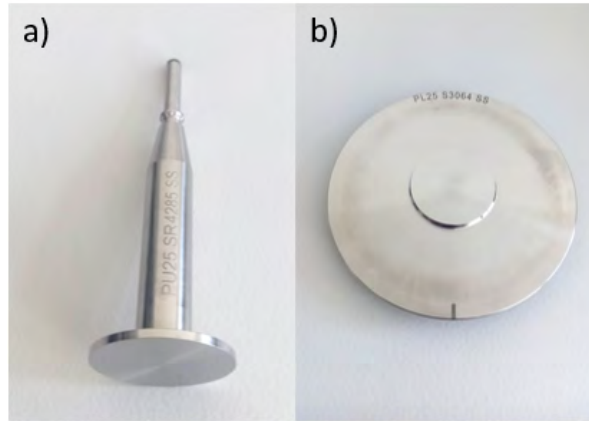


Figure 4.9.: Plate-plate geometry used for amplitude and frequency sweep tests: (a) Upper geometry ($\varnothing 25$ mm); (b) Lower geometry ($\varnothing 25$ mm)

4.2.1. Amplitude sweep test

The amplitude sweep test aims to obtain the length of the LVER. This region is defined as where stress and strain are related linearly. Within this region, the output is directly proportional to the input. In other words, LVER is the area where the storage modulus G' remains constant until a sudden decrease occurs. The LVER ends when linearity is lost. This limit can be set according to how much the storage modulus decreases. [32, 45, 46]. Some standards establish this percentage decrease. In the case of DIN EN 14770, a decrease of 5% is used. However, ASTM D7175, which corresponds to the same type of materials as the previous standard, establishes a value of 10%. Therefore, the decision of the limit value is up to the researcher, depending on which standard is used. For this research, the value established by DIN 51810 is used, which, although it focuses on lubricants, behaves similarly to PBS since they have a non-Newtonian behavior. For this reason, this standard can be taken as a reference for obtaining the results of the amplitude sweep test. Therefore, this research's decreased value of the storage modulus is 10%. [47]. Once the material is outside LVER, it has physical changes and starts the degradation of the internal structure of the sample and rupture mechanisms. [32, 45, 46]

This test maintains a constant frequency value and changes the sweep's amplitude until it surpasses the LVER's limit. Table 4.3. shows the parameters used to perform the amplitude test. It is worth noticing that amplitude in this area refers to the stress or shear strain applied to the material (input).

4.2.2. Amplitude sweep results

Five samples per type of composite material and pure PBS were measured to perform these tests. The graphics below represent the average of those five samples with standard error bars

4. Experimental methodology and results

Table 4.3.: Parameters of the amplitude sweep test

| Amplitude sweep test | |
|----------------------|----------|
| Shear strain (%) | 0.01-100 |
| Frequency (Hz) | 16 |
| Gap (mm) | 1 |
| Temperature (°C) | 25 |

that follow Equation 4.1. To view all the results of the five samples per material, see Appendix A.2. The standard error is the division of the standard deviation by the number of samples (n). The standard deviation was calculated with the software MATLAB with the function of the same name.

$$Standard\ error = \frac{Standard\ deviation}{\sqrt{n}} \quad (4.1)$$

Figure 4.10. and Figure 4.11. show the results of the amplitude sweep test, storage modulus, and loss modulus, respectively. The storage modulus is the most critical parameter because it helps recognize the LVER. In both graphics, the samples are associated with a color to differentiate all the samples. Where pure PBS is represented with blue color and 0%, PBS-20 is associated with color cyan and 20%, PBS-40 with green and 40%, PBS-60 with yellow and 60%, and PBS-80 with orange and 80%.

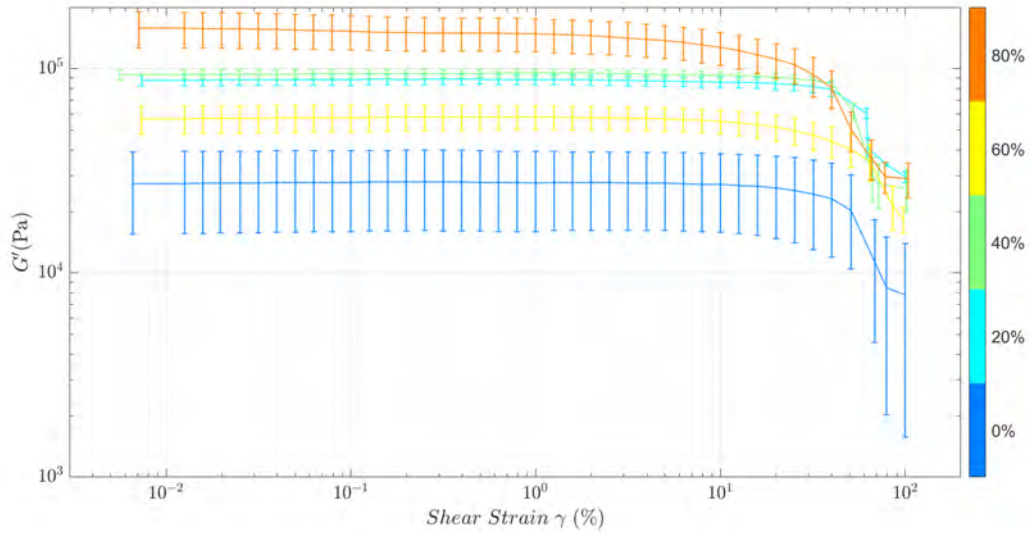


Figure 4.10.: Storage modulus results of amplitude sweep of different amounts of PBS mixed with CIP

It is noted that all the storage moduli are above the value of the loss modulus and that both are constant within the LVER. This result means that the material has a gel-like or solid structure.

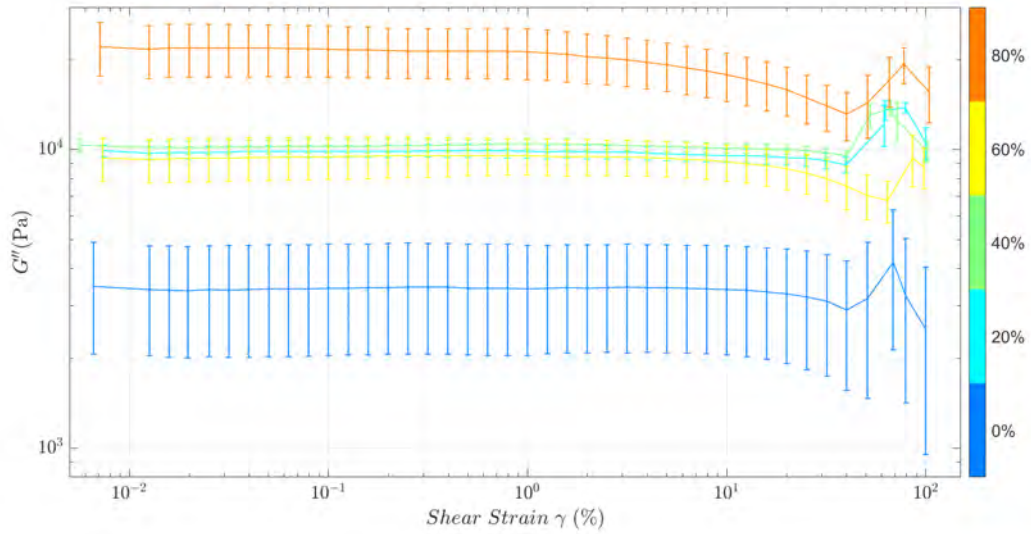


Figure 4.11.: Loss modulus results of amplitude sweep of different amounts of PBS mixed with CIP

All loss moduli exhibit similar behavior: they decrease near the LVER limit, abruptly increase to a peak value, and sharply decrease. The material reflects this behavior as G' decreases and starts to increase sharply. The creation of minor fractures in the material takes place, causing the energy from the environment to be spent in that breakage of the material until G' decreases again, which means that the material starts to flow. The energy is not used on the origin of more fractures. An advantage of PBS is that even when it surpasses the LVER due to its self-healing properties, it could be rejoined again, recovering its initial state. Figure 4.12. shows a before and after amplitude sweep test of the samples where the after picture evidenced that the LVER has been crossed.



Figure 4.12.: Evidence of the surpass of the LVER: before and after the amplitude sweep test respectively

Table 4.4. shows the average values of the limit of the LVER of every sample. It is observed that as the mass fraction of CIP increases, the limit of LVER increases. Nevertheless, this tendency stops when the mass fraction is 60%. This phenomenon suggests a point between 40% and 60% where the limit of the LVER starts to decrease. After that point, the tendency changed, and now, while the mass fraction increases, the limit of the LVER decreases. This

unexpected behavior could be associated with the increase of suspended particles. This amount makes it difficult to maintain a good suspension state, affecting the length of LVER.

A similar case occurs with the values of the storage modulus. The tendency is that the G' increases as the mass fraction increases until 60% CIP is reached. The particularity here is that PBS-60 is the only sample that goes out of trend because the value of PBS-80 has the maximum storage modulus value of 157.8 kPa. This particularity could be associated with the larger distribution of the results of sample PBS-60. However, the trend may be correct due to the behavior of the limit of the LVER. As expected, the stiffest sample is PBS-80 due to the large amount of CIP. A common trend occurs with PBS-20 and PBS-40 increasing its rigidity while the content of particles increases. PBS-60 must surpass a threshold value affecting an inner phenomenon that weakens the material structure, impacting the final properties.

Table 4.4.: Average limit of the LVER of all the samples

| Limit of LVER | | | |
|---------------|------------------|-------------------------------|----------------------|
| Sample | Shear strain (%) | Storage modulus plateau (kPa) | Standard error (kPa) |
| PBS | 31.59 | 27.9 | 11.3 |
| PBS-20 | 39.72 | 88.8 | 6.0 |
| PBS-40 | 39.88 | 95.5 | 3.1 |
| PBS-60 | 20.00 | 57.9 | 7.5 |
| PBS-80 | 3.15 | 157.8 | 26.1 |

4.2.3. Frequency sweep test

The frequency sweep test must be performed within LVER to avoid the inner breakdown of the material and possible errors that could affect the results. That is why this test is performed after the amplitude test. Here, a strain value is established within LVER, and it remains constant while the oscillation frequency increases. [27, 30, 48]. Table 4.5. shows the parameters used in this test. The objective of this test is to observe the material's behavior across the frequency spectrum.

Furthermore, it is possible to obtain the gel point. This point is defined as the point where G' and G'' have the same value, delimiting a change in the behavior. Depending on which modulus is predominant, the behavior will be associated with that. This condition means that if the storage modulus is above the loss modulus, the predominant behavior will be elastic; in the opposite case, the predominant behavior will be viscous. [27, 30, 48]

Table 4.5.: Parameters of the frequency sweep test

| Frequency sweep test | |
|----------------------|----------|
| Shear strain (%) | 0.1 |
| Frequency (Hz) | 0.01-100 |
| Gap (mm) | 1 |
| Temperature (°C) | 25 |

4.2.4. Frequency sweep results

Like in the amplitude sweep test, five samples per kind of material were also tested here. The graphic in this section is the average result of all the samples differentiated by color. PBS is blue with 0%, PBS-20 is cyan with 20%, PBS-40 is green with 40%, PBS-60 is yellow with 60%, and PBS-80 is orange with 80% of CIP in mass fraction. For more information about all the samples' frequency sweep results, see Appendix A.3.

One graphic shows the storage and loss modulus (Figure 4.13.) to observe the gel point properly. All the results follow the same behavior. At low frequencies, $G'' > G'$ where the viscous behavior is predominant until reaching the gel point. Once a frequency higher than the gel point is reached, the predominant behavior changes to elastic. Also, in all the results, the storage modulus starts below the loss modulus, continuously increasing until it reaches the gel point. After that, it increases until a plateau is reached with the final value of G' . This plateau is due to the Si–O:B bonds that have less time to break, retaining the entanglements and restricting the movement of the chains. This phenomenon is reflected in the increase of the material's capability to store energy, reaching a peak constant value where the material behaves like an elastic solid. It should be noted that such results are typical of a viscoelastic liquid.

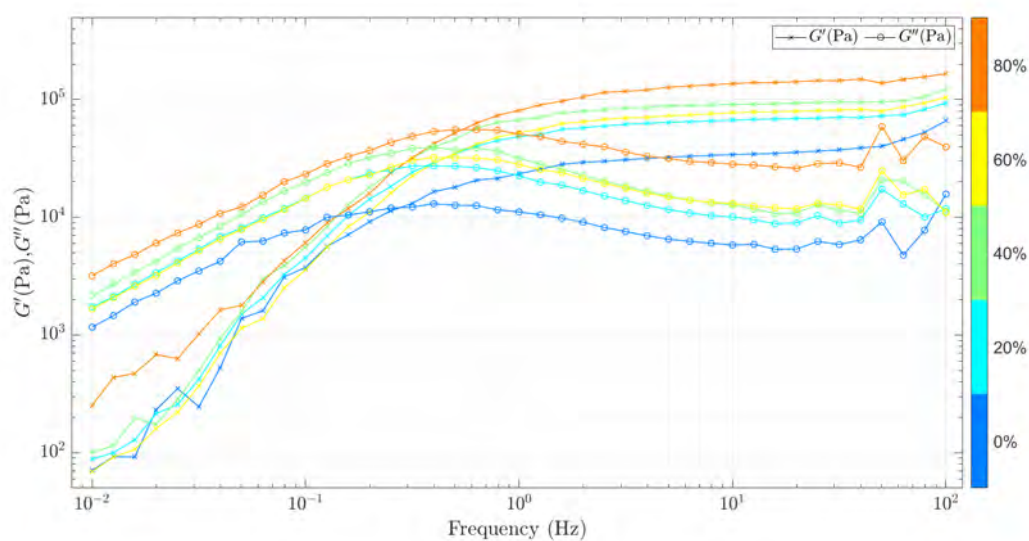


Figure 4.13.: Frequency sweep results of different amounts of PBS mixed with CIP

Instead, the loss modulus begins with higher values over the storage modulus. It also increases but at a lower rate than G' . The maximum value is obtained at the gel point. After that, it decreases until a certain plateau. This behavior reflects the decreasing amount of energy dissipated to the environment. This phenomenon is also explained by the Si–O:B bonds. Due to the quick physical cross-linking, the chains will decrease the motion between each other, reducing the energy used to try to move them. Zhao et al. obtained similar results with a

composite material labeled an SSG made of PBS and CaCO_3 particles. Figure 4.14. shows the results of the frequency and amplitude sweep test. Here, it is possible to observe a behavior similar to that of the material of this research. At low frequencies, G'' is higher than G' , which implies that the behavior in this zone will be predominantly viscous. On the other hand, for high frequencies, G' is above G'' . This means that the shear stiffening effect has occurred. Therefore, the material will have a highly elastic behavior. Although the material studied in Zhao et al. research is similar, the behavior in general terms is the same. [19]. These results lead to the conclusion that the PBS will have the most significant influence on the rheological properties of the composite material and that the particles added to it will have an influence not on the behavior but on the values of G' and G'' . This means that depending on the type of reinforcement particle added, there will be different stiffness and energy storage capacity. However, the shape of the graph will be the same. That is, due to the PBS, it will always behave as a viscous material at low frequencies and as an elastic material at high frequencies.

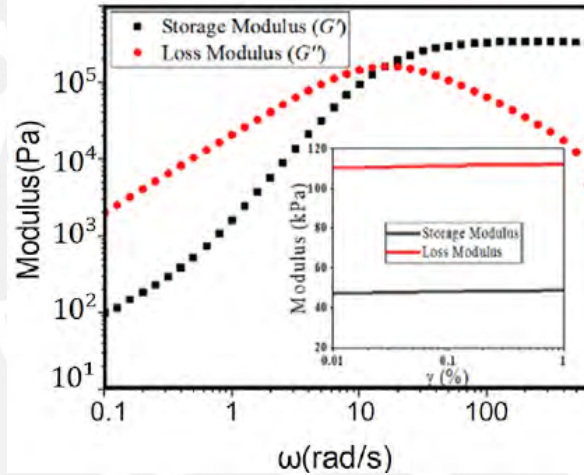


Figure 4.14.: Frequency sweep results SSG reinforced with CaCO_3 particles, extracted from [19]

The same behavior is obtained in the research of Wenbin et al. The frequency sweep test result has the same shape and behavior as that of Zhao et al. and this research. These similar results reinforce the idea that PBS has the most significant influence on the rheological behavior of the composite material. In the case of Wenbin et al., an SSG was also tested, but in that case, no reinforcing particles were added. That is why, in the results of Zhao et al. and the present investigation, final G' values above 10^5 are observed. On the other hand, in the research of Wenbin et al., a value of G' between 10^4 and 10^5 is observed (Figure 4.15.) because it does not have reinforcement particles that increase the material's stiffness. [49]

All storage moduli reach a plateau at high frequencies where the maximum value is obtained. It is observed that as the particle content increases, the maximum value of G' also increases as expected. Nevertheless, PBS-60 reduces its final stiffness, having a plateau of storage modulus

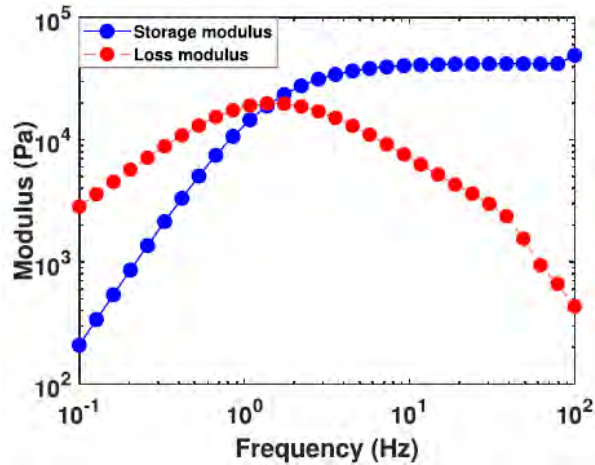


Figure 4.15.: Frequency sweep results SSG, extracted from [49]

below PBS-40 and above PBS-20. This same behavior occurs in the amplitude sweep test. PBS-60 shows a particular behavior compared to the other specimens, indicating that some strange phenomenon happens in that range. Table 4.6. shows the values of the storage and loss modulus of the gel point and the frequency at which it happens. It is noted that the frequency of the gel point moves to the right as the mass fraction of the particles increases. In this case, introducing CIP raises the limit of behavior change, increasing the viscous region of PBS. This behavioral change limit could be related to the rise of rigidity owing to the particles made of iron, a stiffer material. The rise of rigidity gives more resistance to the material, acting like a solid once a threshold is surpassed. That has the impact of needing a higher frequency to trigger the change.

It was observed that particular noise results in a lower frequency for the G' and a higher for the G'' . This noise is related to materials with low viscosity (below 100 mPa.s). This kind of material has a fluid-specific inertia effect. This effect made the noise due to the material not being capable of following the speed of the geometry, creating a delay [50]. Considering these results, it is suggested, for future research, to reduce the amount of material tested by reducing the gap to a narrow space smaller than the one used in this research (1 mm) in order to reduce noise. A possible gap value would be half of that used, i.e., 0.5 mm.

Table 4.6.: Average gel points of all the samples

| Frequency sweep results | | |
|-------------------------|--------------------------|----------------------|
| Sample | Gel point frequency (Hz) | G' and G'' (kPa) |
| PBS | 0.27 | 12.2 |
| PBS-20 | 0.37 | 27.4 |
| PBS-40 | 0.40 | 39.4 |
| PBS-60 | 0.45 | 32.3 |
| PBS-80 | 0.54 | 55.5 |

4.3. Shape change characterization

To measure how the magnetic field affects the material's capability to maintain a given shape, a visual analysis consists of taking photos every 10 minutes for 2.5 hours. In order to have consistent initial shapes for all the samples, a 3D-printed mold in the shape of a semi-sphere with a diameter of 15mm was created. The samples were placed in the mold and trimmed on a small transparent polymer plate. The plate was then positioned between Helmholtz coils arranged near the center over graph paper, which was used as a reference for later analysis. Over this setup is placed a tripod with a camera to take pictures of the sample in the most perpendicular way possible. In order to make sure that the camera is positioned at the right angle, one can use the tripod accessories as a reference. These accessories help align the camera with the transparent polymer surface so that the surface is parallel to the lens. However, sometimes, human error can be due to camera movement while changing the battery between shooting sessions. Figure 4.16. shows the entire configuration of the test.



Figure 4.16.: Shape change test configuration: 1.Camera; 2.Camera tripod; 3.Helmholtz coil

A programmable power supply was used for the pulsating and constant magnetic field. Helmholtz coils were used due to their peculiar behavior. They have a uniform magnetic field in a reduced space near the center of both coils. The Figure 4.17.shows an example of the uniformity of the magnetic field of a Helmholtz coil array. This coil type has identical turns, current, and diameter. For a uniform magnetic field, the coils should be separated by a distance equal to their diameter. [51, 52]

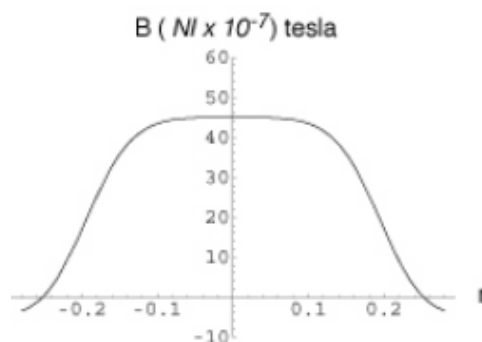


Figure 4.17.: Magnetic field distribution of a Helmholtz coil, extracted from [51]

Due to time constraints, the analysis was only carried out for three samples. PBS is used to observe the pure material acting independently over time. PBS-20 is used to analyze how the introduction of magnetically responsive particles affects the material, which, in this case, is the minimum number of particles added to PBS. Furthermore, PBS-80 is used to analyze if the highest content of particles causes a noticeable change in the material's properties and performance to maintain its initial shape. PBS was left at rest to see how its geometry changed; it was not subjected to a magnetic field because it does not react with these. PBS-20 and PBS-80 were tested with a pulsating magnetic field with 1 and 5 Hz frequencies. Furthermore, they were tested with a constant magnetic field to compare if the pulsating magnetic field is a better way to maintain the initial geometry or is just more efficient to use a constant magnetic field. Finally, they were tested just under the influence of gravity.

Data on the magnitude of the magnetic field have been obtained for 1 and 5 Hz from past research. The programmable power supply gives the coils values of 0 and 32 Volts and 0 and 2 mA. For the constant magnetic field, the values are 32 V and 2 mA. Due to the coils' heating in this condition, they were used for just 1 hour. Figure 4.18. shows the measures of the pulsating magnetic field for 1 Hz reaching a magnitude between 10 and 15 mT on average.

4.3.1. Shape change results

Table 4.7. summarizes the final diameter, area, and diameter increase percentage measurements. All these results were obtained using an image processing program called ImageJ.

A better observation of the results regarding the increase of the diameter over time is shown in Figure 4.19. The increase of PBS-20 and PBS-80 diameter is noted to be bigger than the pure PBS. This phenomenon is caused by the weight of the particles that help the material flow faster due to gravity because now it is bearing the weight of the PBS and CIP. That is why PBS-80 (38.6%) has a slightly higher deformation than PBS-20 (37.1%) under normal conditions only affected by gravity.

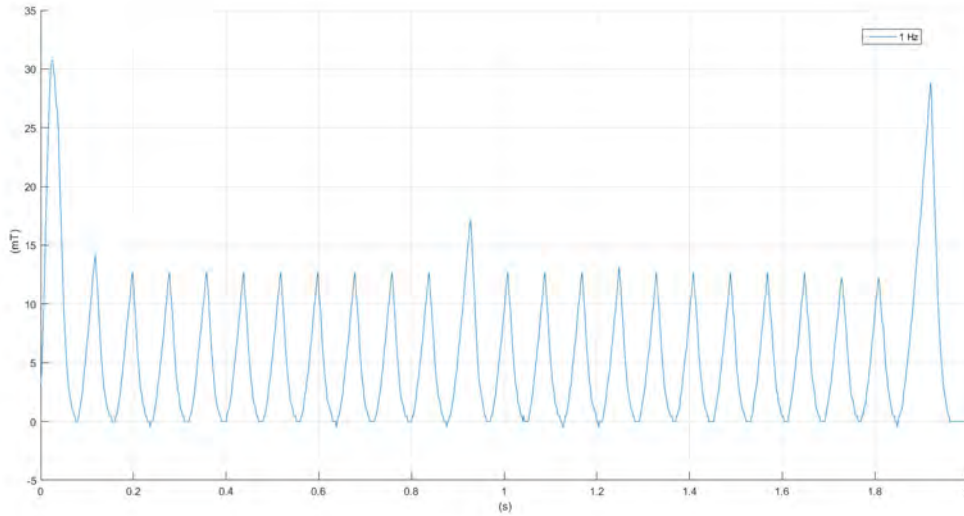


Figure 4.18.: Measure of the pulsating magnetic field for 1 Hz

Table 4.7.: Shape change results

| Shape change summary | | | | |
|----------------------|-------------------------|---------------|-------------------------|------------------|
| Sample | Frequency (Hz) | Diameter (mm) | Area (mm ²) | $\Delta r/r$ (%) |
| PBS-80 | No magnetic field | 20.7 | 336.9 | 38.6 |
| PBS-80 | 1 | 15.7 | 193.9 | 4.4 |
| PBS-80 | 5 | 15.3 | 185.7 | 2.4 |
| PBS-80 | Constant magnetic field | 15.0 | 178.7 | 0.2 |
| PBS-20 | No magnetic field | 20.7 | 337.6 | 37.1 |
| PBS-20 | 1 | 19.5 | 299.4 | 29.6 |
| PBS-20 | 5 | 19.0 | 285.0 | 31.0 |
| PBS-20 | Constant magnetic field | 17.5 | 240.0 | 17.2 |
| PBS | No magnetic field | 17.5 | 239.4 | 13.9 |

Increasing the frequency of the pulsating magnetic field improves maintaining the initial shape by 2.0% in the case of PBS-80. On the other hand, PBS-20 reduced its effect by 1.4%, which was an unexpected behavior. PBS-20 was expected to behave like PBS-80. That is, to increase its ability to maintain a shape as the frequency of the pulsed magnetic field increases. However, this was not the case, so this behavior may be associated with the lower content of particles that hinders their alignment to the magnetic field that appears and disappears quickly. Not all particles could react to the magnetic field (MF) at those rates of change.

Furthermore, the low CIP content does not fulfill the purpose of retaining a desired shape over time. This phenomenon happens because of the CIP. Instead of improving the material's ability to maintain its shape, it causes more deformation when exposed to gravity. This deformation increases when particles exert mechanical loads on the PBS, making its deformation faster when no magnetic field exists. The diameter increase of pure PBS (13.9%) is lower than that of PBS-20 (17.2%). In both samples with CIP, it is observed that the lowest changes were obtained when the magnetic field was constant. As expected, PBS-80 has the highest

capability to maintain a given geometry over time when subjected to a magnetic field. This result is because PBS-80 is the sample with the highest CIP content, so it is more likely that its particles, being in greater quantity, react to the magnetic field.

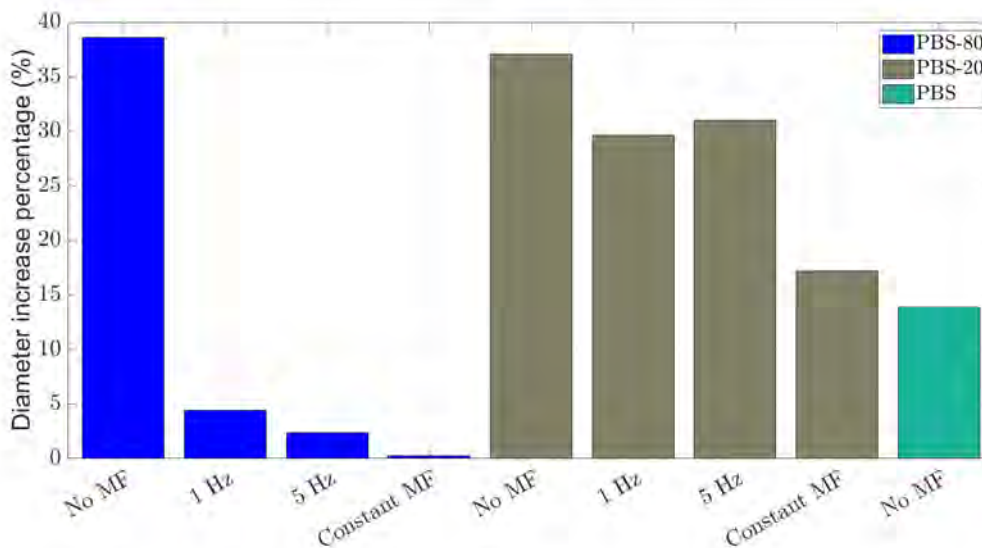


Figure 4.19.: Diameter increase percentage over time

4.4. Further characterization

This section describes the thermogravimetric analysis (TGA), Fourier transform infrared spectroscopy (FTIR), and scanning electron microscope (SEM) analysis. TGA and FTIR were tested in the previously mentioned samples: PBS, PBS-20, and PBS-80. In the case of the SEM, all the samples.

4.4.1. Thermogravimetric analysis

Thermogravimetric analysis is a technique used to measure the degradation of the sample while the temperature increases in a controlled atmosphere. This test consists of a sample crucible supported by a highly precision balance. These are inside a furnace that will increase the temperature at a controlled rate, under a desired atmosphere, until a maximum temperature. The mass of the sample is monitored all the time the experiment is developing. [53]. This case used simultaneous thermogravimetry from the brand Netzsch model STA 449 F3 Jupiter. This device can be programmed to follow standard procedures. ASTM E1131, Standard Test Method for Compositional Analysis by TGA, was followed in this case. Table 4.8. shows the parameters used for this test.

Table 4.8.: TGA parameters followed by ASTM E1131 [54]

| TGA parameters | | |
|---------------------|-------|--------|
| Parameter | Value | Unit |
| Flow rate | 50 | mL/min |
| Heating rate | 10 | °C/min |
| Gas switchover | 600 | °C |
| Maximum temperature | 750 | °C |

The atmosphere is always nitrogen until the gas switchover temperature is reached. Once this temperature is surpassed, oxygen flow enters the chamber, removing the nitrogen [54]. All the above parameters and conditions were extracted from ASTM E1131. Since PBS is an elastomer, the parameters for this type of polymer within the standard were used.

Thermogravimetric analysis results

All the graphics in this section present two Y-axis where the one on the left represents the percentage of mass change of the sample, and the other on the right shows the derivative of the mass percentage. The X-axis shows the temperature. The derivative is used to obtain the highest rate of change in the degradation of the material when losing a high amount of weight.

Figure 4.20. shows the results of pure PBS. The red line represents the region where the atmosphere is pure nitrogen; the blue line is when oxygen is in the atmosphere. In this case, the highest peak where the mass change is at 487,5 °C. This temperature is selected as the degradation temperature of PBS. It does not react when the change from nitrogen to oxygen occurs because this sample has no components that can react with the oxygen atmosphere. There are three main slopes present in the graph. The first is due to moisture loss with a 0.78% mass loss. Then follows the second slope between 367 °C and 430 °C. The mass loss on that slope is 10.82%. Finally, the third slope is from 430 °C to the end of the test, in this case, 850 °C due to the test procedure of the Pontificia Universidad Católica del Perú (PUCP) university laboratory.

The final temperature differs from the standard; however, these are procedures established by the university and will not affect the final remains as the material has already been degraded. In this slope, the mass loss is 85.59%, and almost all the weight burns in this region. These two steeper slopes could be related to the physical reticulation that permanently binds and breaks. The temperature increases the probability of breaking the bonds, resulting in a PBS that acts more like a viscous liquid because of the energy of the high temperatures. After the test, the rest of the mass corresponds to 3% of the initial mass, a high value compared to other polymers. These rests could be related to the high content of oxygen and silicon in PBS. Silicon has a boiling temperature of 3265 °C, so this element in the PBS will not be degraded or eliminated in vapor due to the final temperature reached in the test [55]. Miandad et al. present TGA results for different common polymers such as polystyrene (PS), polyethylene (PE), polypropylene (PP), and polyethylene terephthalate (PET). These show a

final mass of about 5% for PS and close to 0% for the other polymers. PS has a higher final mass due to carbonization. However, in general, the final mass of the polymers is close to 0%. [56]. It should be noted that PBS has a slightly higher temperature resistance compared to common polymers that degrade 300 °C and 470 °C, as can be seen in Figure 4.21. [56]

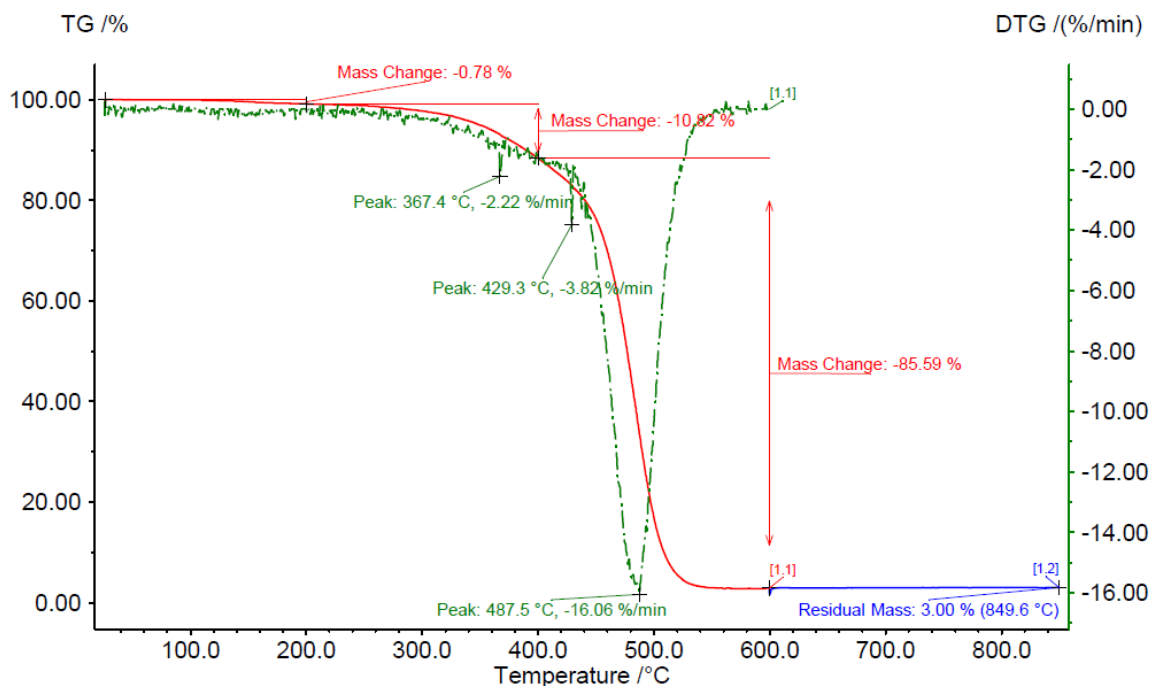


Figure 4.20.: PBS TGA results

Figure 4.22. shows the results of PBS-20. In this case, PBS-20 has a slight slope for moisture loss equal to PBS. This similar behavior is because the more significant amount of mass is from the PBS, so its characteristics predominate. However, when the switch-over temperature is reached, the mass decreases more as the oxygen atmosphere enters the chamber, and nitrogen remains.

After the switch-over temperature, the residual CIP particles react with the oxygen atmosphere, producing an oxidative reaction, so the mass increases from 22.47% to 29.71%. The final residual mass is 22.47% of the initial mass, which means that the mixture process of PBS with CIP was successful because the theoretical mass fraction was 20%. The degradation temperature is 503 °C, and as expected, the addition of CIP improves the overall temperature resistance of the material as the particles have higher temperature resistance due to their carbon and iron content. The mass loss was 77.53% for the degradation temperature.

Figure 4.23. shows the results of PBS-80. Here, the change of atmosphere was removed because it could affect the high precision balance of the TGA device due to the high content of particles

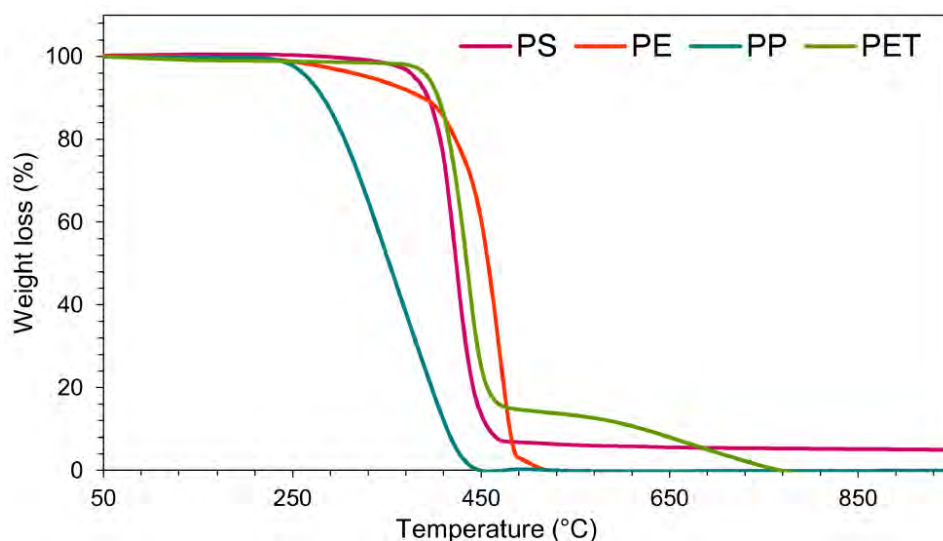


Figure 4.21.: PS, PE, PP, and PET TGA results from [56]

that will react with the oxygen. As noted with the other two samples, adding CIP increases the resistance to temperature. The degradation temperature rises to 525 °C. This increase is because of the significant content of particles; the polymer, in this case, is just 20% of the mass. The particles are made of iron, which resists higher temperatures than a polymer. The mass change in this region was 20.67%, leaving a residual mass of 79.33%. Nevertheless, from 700 °C and above, the residual mass increases to 80.67%. This phenomenon could be related to the release of oxygen from the siloxane backbone, which reacts with iron, causing a mild oxidative reaction. Due to the nature of PBS, both PBS-20 and PBS-80 maintain the two main slopes due to dynamic physical crosslinking. Ran et al. presented a similar behavior for a mixture of PBS with ammonium polyphosphate (APP). In the TGA result, a slight decrease is observed at the beginning due to humidity and then two steep slopes as the temperature increases. [57]. These results reinforce the idea that PBS has two degradation curves.

4.4.2. Fourier transform infrared spectroscopy

Fourier transform infrared spectroscopy is a technique where infrared radiation passes through a sample. The sample absorbs some of the radiation (absorbance), while other amounts pass to the other face of the material (transmittance). A sensor is placed to measure the quantity of radiation. The particularity is that the molecules absorb the radiation depending on the bond and elements it has. Due to bonds and functional groups absorbing different frequencies, every molecule has its spectrum, like a fingerprint to a human. The Fourier transform is a mathematical function that allows the transformation of the spectrum to the frequency of the wave based on time. So, the device's output is now an infrared spectrum graph that could be interpreted. Within FTIR devices is a component named attenuated total reflectance (ATR),

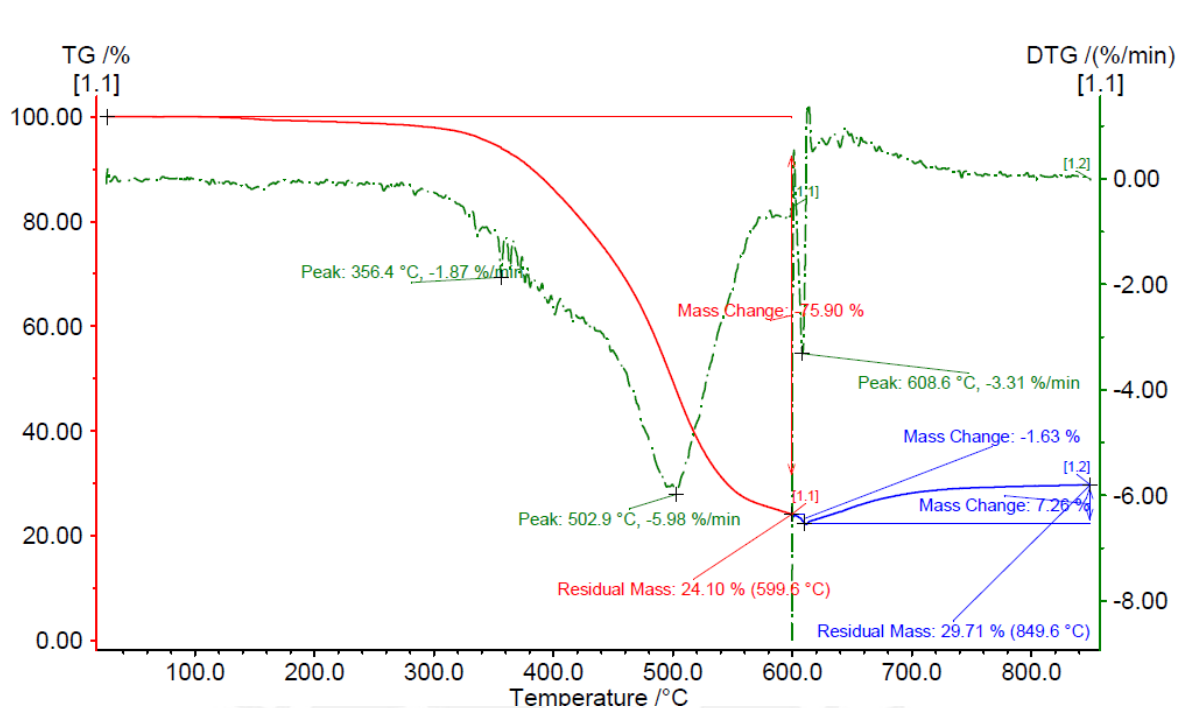


Figure 4.22.: PBS-20 TGA results

which is based on total internal reflection. This reflection is recognized by interacting with two optical media with different refractive indices. At a certain angle, the light is totally reflected. The ATR uses a crystal as a medium to reflect the light between the sample and it. This device improves the refraction in some samples that are not highly reflective. [58, 59]. In this case, the device used is a Bruker model Tensor27 TGA-IR.

Fourier transform infrared spectroscopy results

Figure 4.24. shows the results obtained where PBS is the blue line, PBS-20 is black, and PBS-80 is pink. As noted, the absorbance of PBS and PBS-20 are similar. The amount of radiation absorbed increases a little in the sample PBS-20. The only peak outside the fingerprint region is 2962 cm^{-1} , belonging to the C–H single bond stretch [60]. Within the fingerprint region are characteristic peaks, 1257 cm^{-1} , related to Si–C, a characteristic bond of PDMS [61]. The range between 1009 and 1079 cm^{-1} is related to Si–O–Si bonds. This range confirms the existence of structure type III, mentioned in Section 2.3, which is a cyclical PBS [61]. Finally, the most important bonds related to B–O–Si bonds are observed in the 661 to 786 cm^{-1} [61]. This characteristic bond proves the correct polymerization process of PDMS with BA.

It should be noted that some other bonds overlap in that zone because there are regions without peaks, making a continuous area. This one is more pronounced in the band of 500 to 660 cm^{-1} in the PBS-80 sample, maybe related to the iron and carbon content of the particles. The Si–C peak is the only one that maintains its value in the three samples. The Si–O–Si bonds are

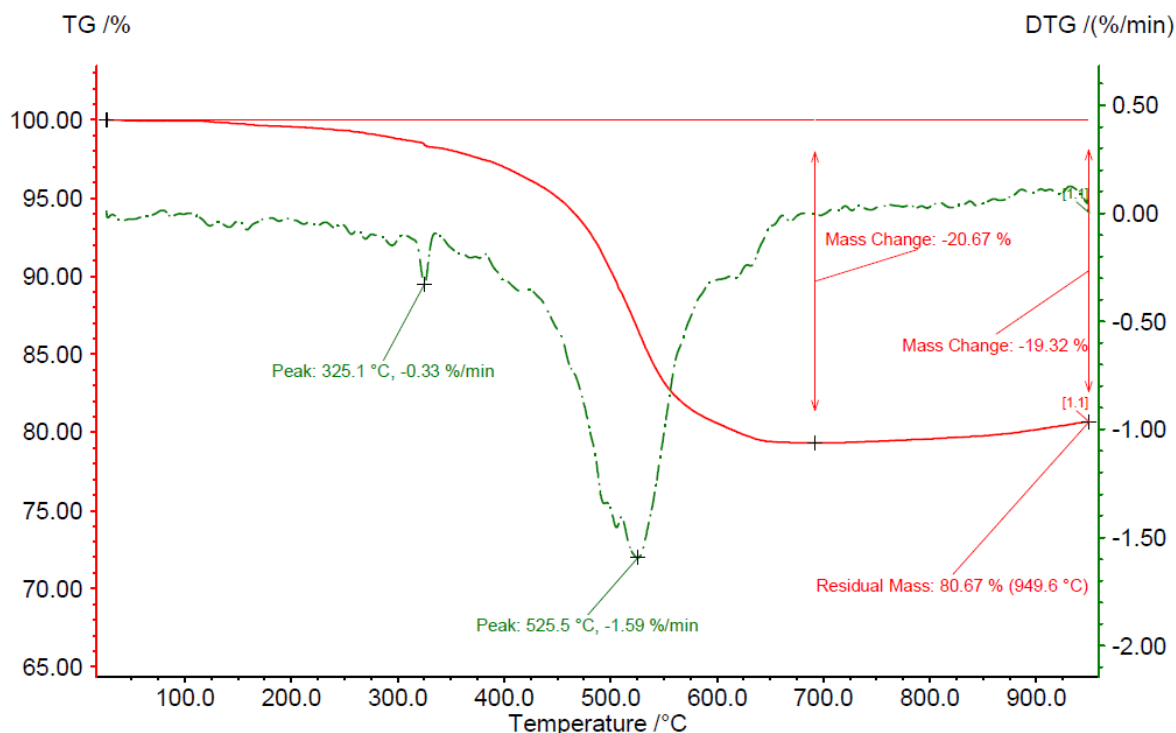


Figure 4.23.: PBS-80 TGA results

present in a higher quantity in samples PBS and PBS-20 due to the amount of PBS in those mixtures. PBS-80 has a reduced absorption due to it having higher particle content. The same occurs with the B–O–Si bonds except in the range of 500 to 660 cm^{-1} , with an overlapping region.

4.4.3. Scanning Electron Microscope

A scanning electron microscope is a microscope that uses electrons to generate an image instead of light, like in optical microscopes. They stand out for the magnifications they can achieve and the higher resolution. A beam of electrons is produced by a cathode, usually made of tungsten filament. The electron beam goes through a magnetic lens that helps focus, moving them up and down, like in the typical microscope lens. The electron beam hits the sample, and all the reflected electrons are x-rays, secondary electrons, Auger electrons, and back-scattered electrons. The sample is placed in a chamber with a vacuum to avoid the presence of strange particles like dust. The detector near the sample recollects the information from those electrons and converts them into a signal sent to a screen. [62]. In this case, an FEI Quanta 650 SEM was used. As the samples are polymers, a previous treatment is needed to ensure the electrical conductivity to acquire correct images. Given this, a low vacuum mode is used, introducing a water vapor atmosphere into the SEM sample chamber to improve the conductivity of the

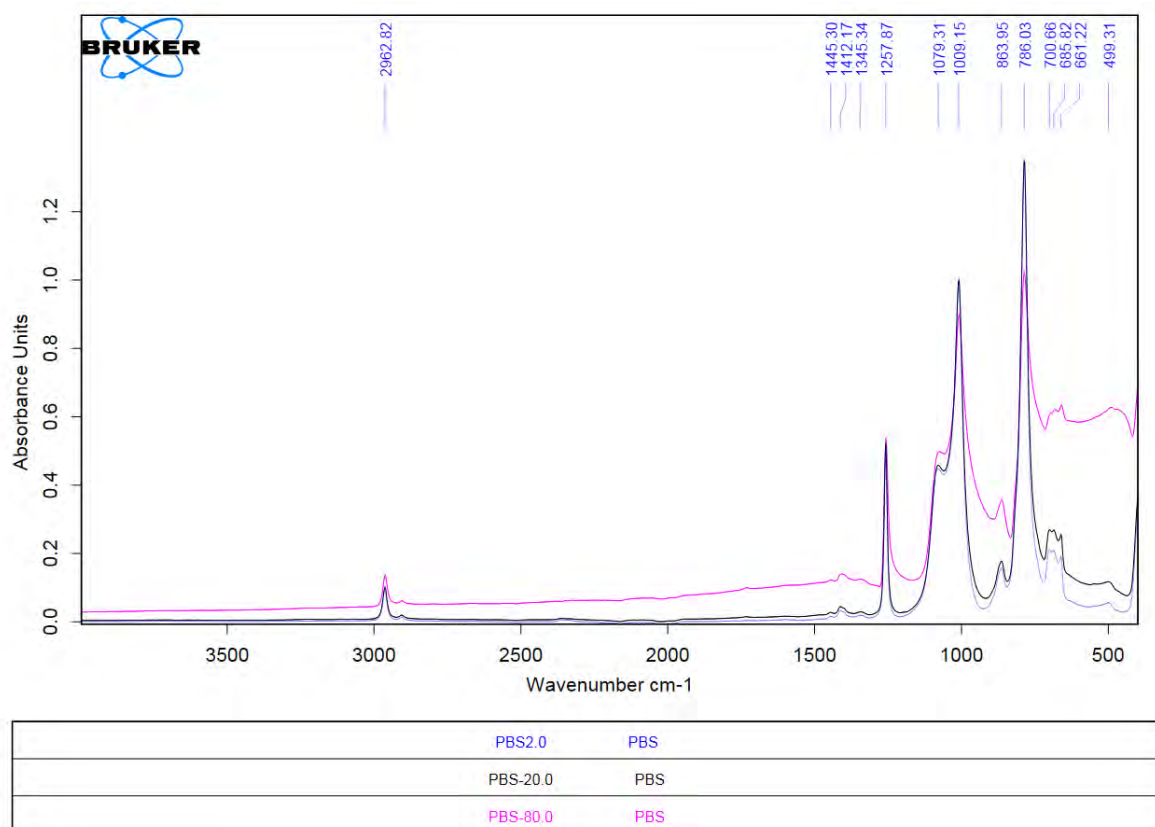


Figure 4.24.: FTIR results of PBS, PBS-20 and PBS-80

electrons and on the sample surface to avoid the accumulation of electrons in certain areas due to the low or lack of electric conductivity.

Scanning Electron Microscope Images

Figure 4.25. shows the PBS surface at 500, 1000, 2500, and 5000 magnifications, respectively. Some particles with random shapes around 1.5 to 2.8 μm are observed. These particles are different from those of CIP, which are spherical, so it can be deduced that these irregularly shaped particles are remnants of BA. As mentioned above, a higher percentage of BA has been added to the stoichiometric one to accelerate the PBS synthesis process and increase the interactions between PDMS and BA. Therefore, the presence of these particles in the material is expected.

Figure 4.26. shows the images of PBS-20. The low amount of CIP particles can be observed in these images, especially in the image at 10000 magnifications. Here, it can be seen that only some of the area has been filled by the particles compared to the later images of the samples with higher CIP content. In addition, some CIP particles with dimensions between 1.3 and 2.1 μm are observed. There are some presences of particles with arbitrary forms and some holes

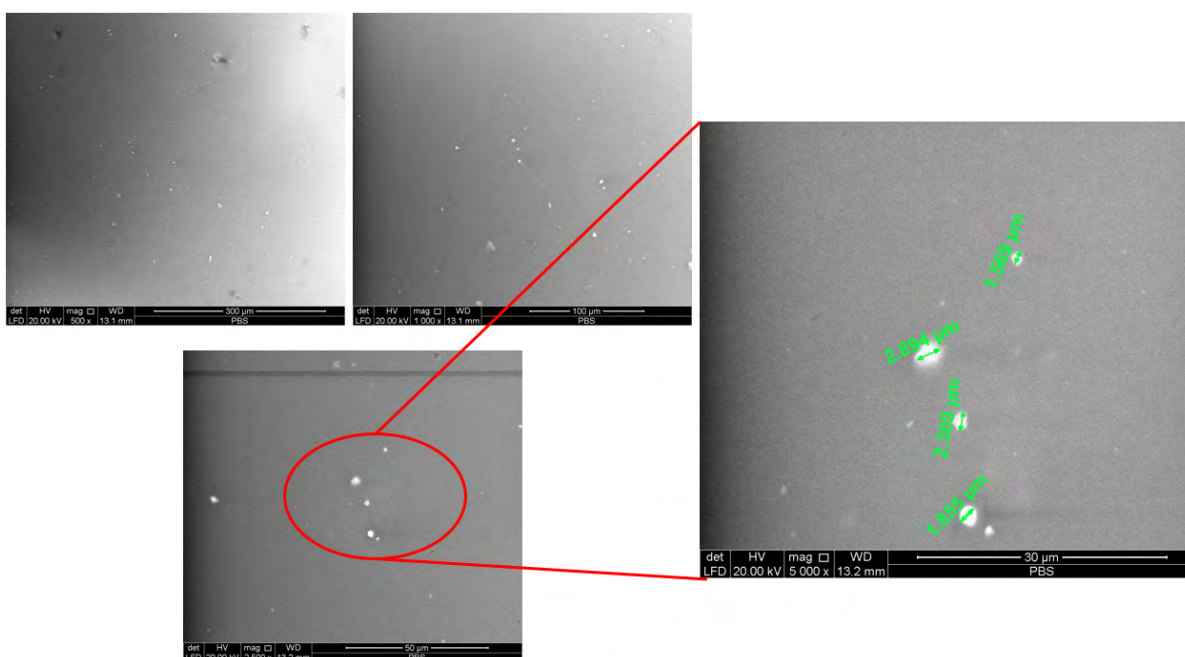


Figure 4.25.: SEM images of pure PBS: 500; 1000; 2500; 5000 magnifications

(black areas). The presence of these holes can be related to the vacuum of the SEM chamber that causes the generation of bubbles in the PBS. At a certain point, these bubbles burst and leave holes in these areas. They can also be caused by the irregularity of the PBS surface because, when the samples were placed, they were only crushed manually to obtain a smooth and expanded surface.

Figure 4.27. presents a higher quantity of particles well spread along the material. Here, the particles are spherical and have dimensions between 1.1 and 1.9 μm . The traces of BA were present, too.

Figure 4.28. shows how the particles are covering more area of the surface. The presence of the CIP is highly noted. However, the image at 10000 magnification shows a distortion that resembles an image taken of a moving object. This phenomenon is called the charging effect and is common in SEM when analyzing insulating materials or materials with low electrical conductivity [63]. The electrons in the beam accumulate in the insulating areas and distort the electron beam that continues to fall on the surface [63]. These accumulated electrons on the surface deflect the electron beam so that the image looks like it has been dragged [63]. The dimensions of the particles are between 1.4 and 3.2 μm .

Figure 4.29. shows a high area covered by the CIP well distributed through the material. The stability of the images is superior to others due to the high particle content. This means that it has, compared to the other samples, a higher electrical conductivity. This is due to the

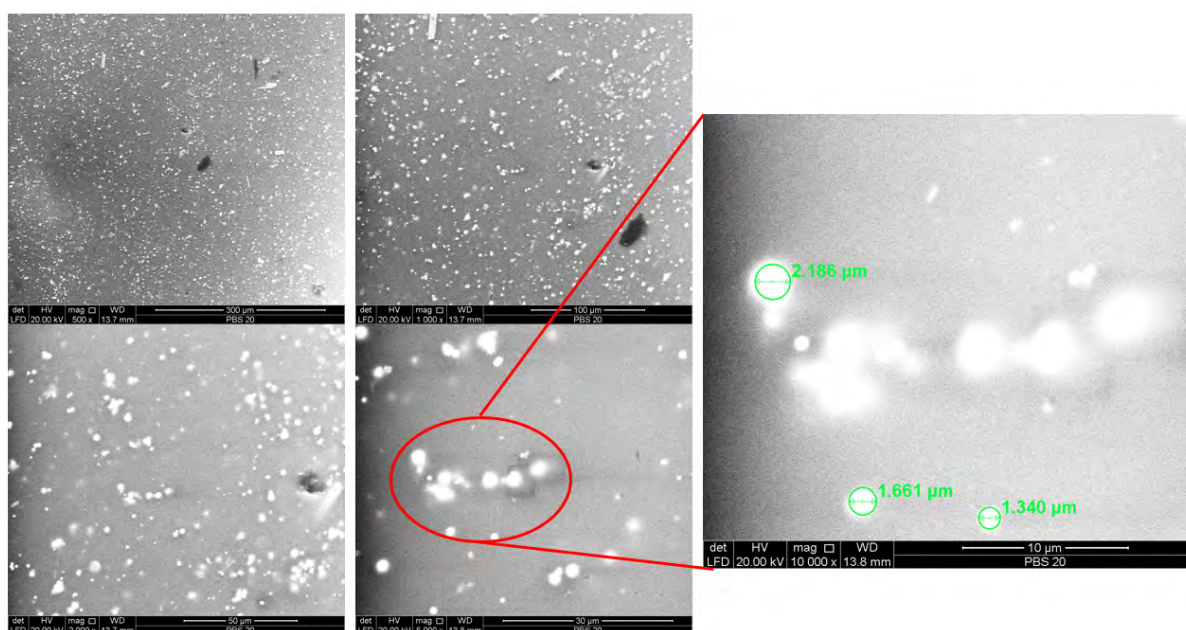


Figure 4.26.: SEM images of PBS-20: 500; 1000; 2000; 5000; 10000 magnifications

higher particle content because it contains iron, a metal with higher electrical conductivity than PBS. Being present in 80% of the mass, its physical properties favor the conductivity of the composite material. Some holes are present, too. The particles in these images are between 1.1 to 3.1 μm . There are also remnants of BA with irregular shapes different from the shape of the CIP particles with a rather spherical shape.

All the particles are well distributed, there are no agglomerations, and the particles are suspended in the matrix of PBS. This suspension state demonstrates, together with the FTIR test, that the particles are not reacting with the polymer. They also reinforce the feasibility of mixing PBS with CIP particles after PBS synthesis. As for the size of the CIP particles, they range from 1.1 to 3.2 μm in size. These values are somewhat far from what was expected, between 3.8 and 5.3 μm . However, the scale is still at the micron level, so it is known that microparticles are being used for this composite material.

4. Experimental methodology and results

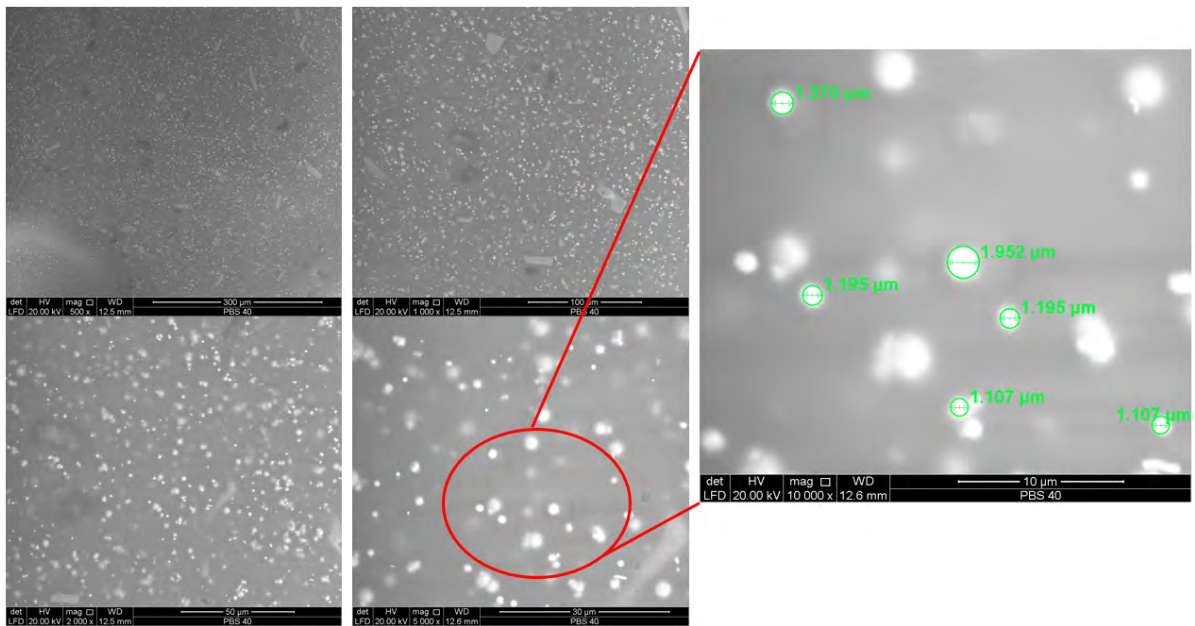


Figure 4.27.: SEM images of PBS-40: 500; 1000; 2000; 5000; 10000 magnifications

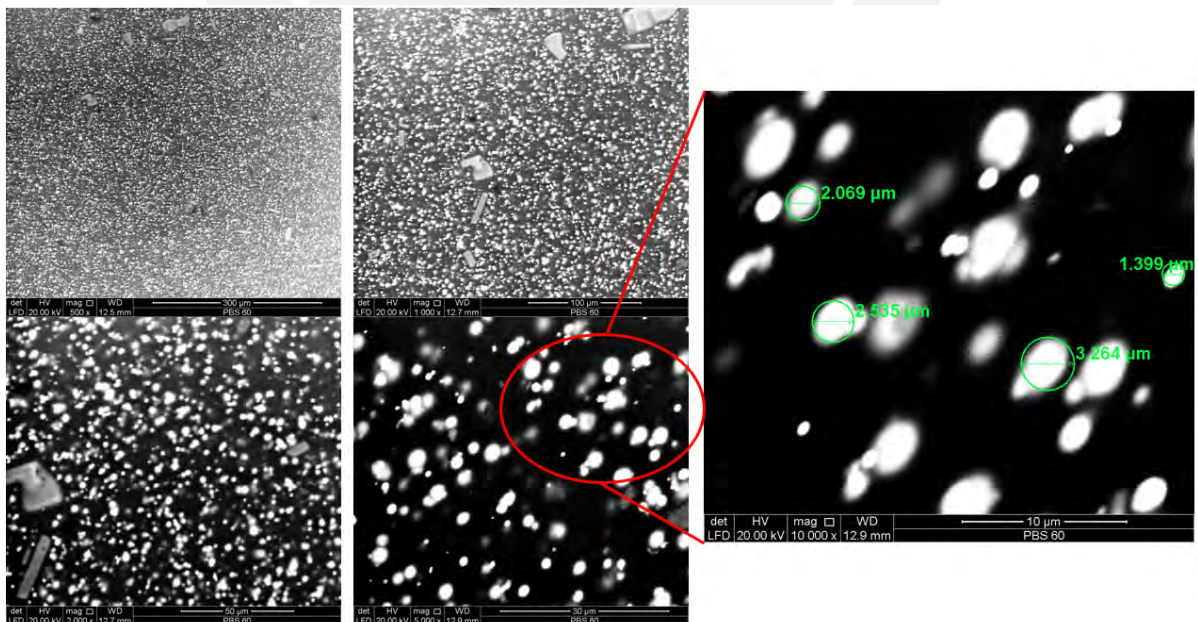


Figure 4.28.: SEM images of PBS-60: 500; 1000; 2000; 5000; 10000 magnifications

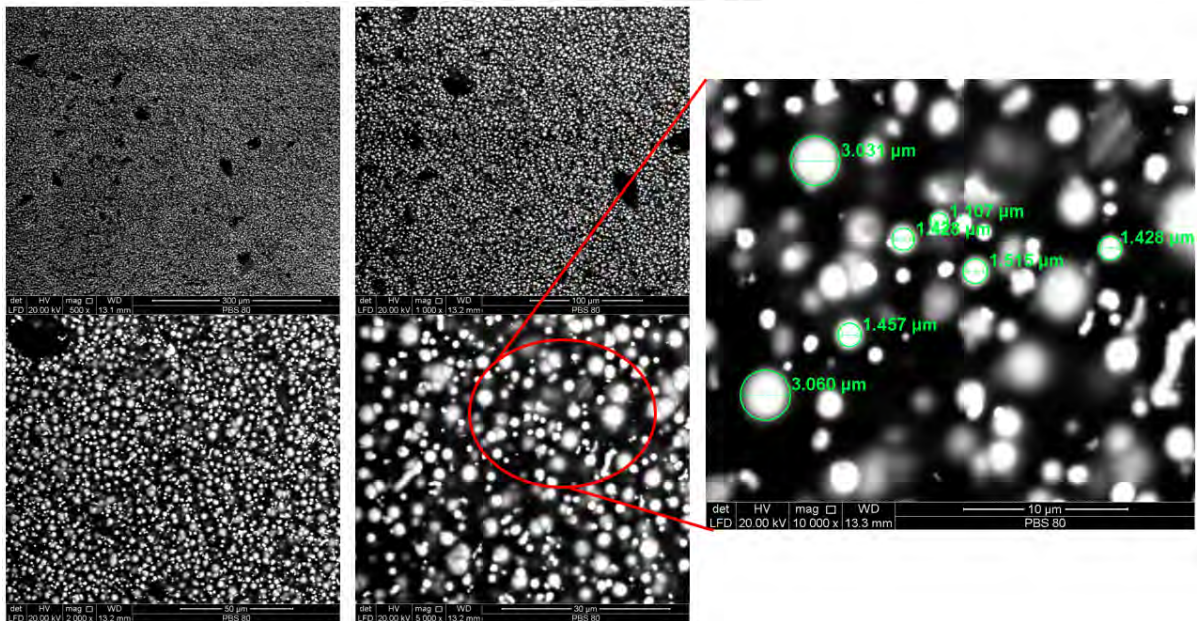


Figure 4.29.: SEM images of PBS-80: 500; 1000; 2000; 5000; 10000 magnifications

5. Conclusions and future investigations

This chapter summarizes the investigation's conclusions, and an outlook for future investigations is presented in the field of smart materials and shear stiffening gels related to soft robotics. Also, some things could be improved with the tests or pending results due to the time limit.

5.1. Conclusions

The material prepared with PBS and CIP successfully demonstrated that it could maintain its shape over time when subjected to a magnetic field. How the magnetic field is delivered increases or decreases its ability to maintain its shape over time. The constant magnetic field demonstrates a highly maintaining shape effect with just 0.2% of diameter increasing over 1 hour. The sample with those results is labeled as PBS-80 with 80% content of CIP.

It increases its stiffness when the content of particles increases. However, there is an unexpected phenomenon between PBS-40 and PBS-60 in which the stiffness decreases and increases again once a specific value between 40 and 60% of mass is exceeded. The stiffness was expected to increase as the particle content increased following the initial trend. PBS-80 shows the highest stiffness with a value of 157.8 kPa. Also, it shows the need for a higher frequency to trigger the change of behavior from viscous to elastic due to the Si–O:B bonds that restrict the slide of the chains of PBS, making it capable of storing more significant amounts of energy.

The distribution of the particles along the material is homogeneous; there were no traces of agglomerations, and the particles possess a spherical shape that certainly does not react with PBS. The FTIR results show that the composite material possesses Si–O–Si bonds, demonstrating the existence of the structure type III with a cyclical shape.

Finally, the TGA shows how the material degrades with two different slopes, not counting the loss of moisture, which could be related to the weakening of the physical cross-linking due to Si–O:B. In addition, PBS has a higher degradation temperature than other commonly used polymers. The particles could react with the oxygen with a high response at high temperatures, increasing the mass and considering the possibility of oxidation of iron present in the particles.

All these properties place the composite material as a promising material for the soft robotics field due to its softness representing a low risk for the safety hazard of the product and persons around, its high resistant temperature, the shape maintaining capability under magnetic fields to handle fragile and delicate materials, its capability to absorb impacts to serve as a safety component and more.

5.2. Future investigations

It is pending to investigate mass fractions of CIP between 40% and 60% through rheological tests to analyze what is happening in that range that causes the reduction of stiffness. This pending investigation is to know which phenomenon causes this trend change in the stiffness of PBS with CIP particles. Also, the same situation with the shape change characterization is pending to analyze the same samples and investigate what could happen if the magnetic field alternates from a positive to a negative value. It is desirable to know whether changing the direction of the magnetic field can increase the shape-holding ability of PBS with CIP particles over time. This condition, to be checked, would help to ensure that the given shape is preserved over time and avoids unwanted deformation when changing shape.

As a suggestion, it is mentioned that it is possible to improve the results of the rheological characterization by reducing the gap height and increasing the area of the plates to eliminate the noise present at the ends of the graphical results of the frequency sweep test [50].

This composite material shows promising properties for soft robotics. It opens the door to its implementation in various parts, such as grippers. The latter are continuously improved, and scientific research lately focuses on biomimetics and biohybrids. Although this material does not have biohybrids, it can increase its stiffness to a magnetic field to simulate the functioning of muscles in humans. Future research can implement PBS with CIP particles in tweezers to analyze its performance in gripping delicate objects. [64]. Another possibility is to analyze its effectiveness as an artificial muscle and check if it can reduce the traction travel limit due to its viscoelastic characteristic that allows the use of complex shapes [65].

Another prospect is to add piezoelectric particles and analyze whether they could improve the shape-keeping capability or be applied in the field of flexible smart devices thanks to their ability to conduct electricity and change their rigidity in the face of a controlled electric field [11].

Bibliography

- [1] WHITESIDES, G. M.: Soft Robotics. In: *Angewandte Chemie (International ed. in English)* 57.16 (2018), pp. 4258–4273. DOI: 10.1002/anie.201800907.
- [2] MAJIDI, C.: Soft–Matter Engineering for Soft Robotics. In: *Advanced Materials Technologies* 4.2 (2019). ISSN: 2365-709X. DOI: 10.1002/admt.201800477.
- [3] U.S. DEPARTMENT OF LABOR: OSHA Technical Manual (OTM) Section IV:Chapter 4: Industrial Robot Systems and Industrial Robot System Safety. Ed. by U.S. DEPARTMENT OF LABOR. U.S. Department of Labor, 2021.
- [4] COYLE, S.; MAJIDI, C.; LEDUC, P., and HSIA, K. J.: Bio-inspired soft robotics: Material selection, actuation, and design. In: *Extreme Mechanics Letters* 22 (2018), pp. 51–59. ISSN: 23524316. DOI: 10.1016/j.eml.2018.05.003.
- [5] DROZDOV, F. V.; MANOKHINA, E. A.; VU, T. D., and MUZAFAROV, A. M.: Polyborosiloxanes (PBS): Evolution of Approaches to the Synthesis and the Prospects of Their Application. In: *Polymers* 14.22 (2022). DOI: 10.3390/polym14224824.
- [6] KURKIN, A.; LIPIK, V.; TAN, K. B. L.; SEAH, G. L.; ZHANG, X., and TOK, A. I. Y.: Correlations Between Precursor Molecular Weight and Dynamic Mechanical Properties of Polyborosiloxane (PBS). In: *Macromolecular Materials and Engineering* 306.11 (2021). ISSN: 1438-7492. DOI: 10.1002/mame.202100360.
- [7] TANG, M.; WANG, W.; XU, D., and WANG, Z.: Synthesis of Structure-Controlled Polyborosiloxanes and Investigation on Their Viscoelastic Response to Molecular Mass of Polydimethylsiloxane Triggered by Both Chemical and Physical Interactions. In: *Industrial & Engineering Chemistry Research* 55.49 (2016), pp. 12582–12589. ISSN: 0888-5885. DOI: 10.1021/acs.iecr.6b03823.
- [8] LIU, S.; WANG, S.; SANG, M.; ZHOU, J.; ZHANG, J.; XUAN, S., and GONG, X.: Nacre-Mimetic Hierarchical Architecture in Polyborosiloxane Composites for Synergistically Enhanced Impact Resistance and Ultra-Efficient Electromagnetic Interference Shielding. In: *ACS nano* 16.11 (2022), pp. 19067–19086. DOI: 10.1021/acsnano.2c08104.
- [9] TANG, M.; ZHENG, P.; WANG, K.; QIN, Y.; JIANG, Y.; CHENG, Y.; LI, Z., and WU, L.: Autonomous self-healing, self-adhesive, highly conductive composites based on a silver-filled polyborosiloxane/polydimethylsiloxane double-network elastomer. In: *Journal of Materials Chemistry A* 7.48 (2019), pp. 27278–27288. ISSN: 2050-7488. DOI: 10.1039/c9ta09158k.

- [10] WU, T. and CHEN, B.: Synthesis of Multiwalled Carbon Nanotube-Reinforced Polyborosiloxane Nanocomposites with Mechanically Adaptive and Self-Healing Capabilities for Flexible Conductors. In: *ACS applied materials & interfaces* 8.36 (2016), pp. 24071–24078. DOI: 10.1021/acsami.6b06137.
- [11] ZHAO, J.; JIANG, N.; ZHANG, D.; HE, B., and CHEN, X.: Study on Optimization of Damping Performance and Damping Temperature Range of Silicone Rubber by Polyborosiloxane Gel. In: *Polymers* 12.5 (2020). DOI: 10.3390/polym12051196.
- [12] ZHAO, Z.; LIU, F.; YANG, X.; ZHANG, D.; LUAN, S.; XU, D., and SHI, T.: Structure and impact properties of a thermoplastic elastomer/silly putty blend. In: *Polymer International* 71.3 (2022), pp. 328–337. ISSN: 0959-8103. DOI: 10.1002/pi.6333.
- [13] ZHAO, C.; WANG, Y.; GAO, L.; XU, Y.; FAN, Z.; LIU, X.; NI, Y.; XUAN, S.; DENG, H., and GONG, X.: High-Performance Liquid Metal/Polyborosiloxane Elastomer toward Thermally Conductive Applications. In: *ACS applied materials & interfaces* 14.18 (2022), pp. 21564–21576. DOI: 10.1021/acsami.2c04994.
- [14] GORODKIN, S. R.; JAMES, R. O., and KORDONSKI, W. I.: Magnetic properties of carbonyl iron particles in magnetorheological fluids. In: *Journal of Physics: Conference Series* 149 (2009), p. 012051. DOI: 10.1088/1742-6596/149/1/012051.
- [15] WANG, Y.; WANG, S.; XU, C.; XUAN, S.; JIANG, W., and GONG, X.: Dynamic behavior of magnetically responsive shear-stiffening gel under high strain rate. In: *Composites Science and Technology* 127 (2016), pp. 169–176. ISSN: 02663538. DOI: 10.1016/j.compscitech.2016.03.009.
- [16] DING, L.; ZHANG, S.; WANG, Q.; WANG, Y.; XUAN, S.; GONG, X., and ZHANG, D.: Self-healing and printable elastomer with excellent shear stiffening and magnetorheological properties. In: *Composites Science and Technology* 223 (2022), p. 109430. ISSN: 02663538. DOI: 10.1016/j.compscitech.2022.109430.
- [17] FAN, X.; WANG, S.; ZHANG, S.; WANG, Y., and GONG, X.: Magnetically sensitive nanocomposites based on the conductive shear-stiffening gel. In: *Journal of Materials Science* 54.9 (2019), pp. 6971–6981. ISSN: 0022-2461. DOI: 10.1007/s10853-019-03360-8.
- [18] WANG, Y.; DING, L.; ZHAO, C.; WANG, S.; XUAN, S.; JIANG, H., and GONG, X.: A novel magnetorheological shear-stiffening elastomer with self-healing ability. In: *Composites Science and Technology* 168 (2018), pp. 303–311. ISSN: 02663538. DOI: 10.1016/j.compscitech.2018.10.019.
- [19] ZHAO, C.; GONG, X.; WANG, S.; JIANG, W., and XUAN, S.: Shear Stiffening Gels for Intelligent Anti-impact Applications. In: *Cell Reports Physical Science* 1.12 (2020), p. 100266. ISSN: 26663864. DOI: 10.1016/j.xcrp.2020.100266.

- [20] KAMILA: INTRODUCTION, CLASSIFICATION AND APPLICATIONS OF SMART MATERIALS: AN OVERVIEW. In: American Journal of Applied Sciences 10.8 (2013), pp. 876–880. ISSN: 1546-9239. DOI: 10.3844/ajassp.2013.876.880.
- [21] KÖK, M.; QADER, İ. N.; DAĞDELEN, F., and AYDOĞDU, Y.: Akıllı Malzemeler üzerine derleme: araştırmalar ve uygulamaları. In: El-Cezeri Fen ve Mühendislik Dergisi (2019). ISSN: 2148-3736. DOI: 10.31202/ecjse.562177.
- [22] PIERRI, J.: The fiber optic. Ed. by PIERRI, J. 2010.
- [23] CASINI, M.: Advanced materials for architecture. In: Smart Buildings. Elsevier, 2016, pp. 55–104. ISBN: 9780081009727. DOI: 10.1016/B978-0-08-100635-1.00002-2.
- [24] KOIKE, Y. and ASAI, M.: The future of plastic optical fiber. In: NPG Asia Materials 1.1 (2009), pp. 22–28. ISSN: 1884-4049. DOI: 10.1038/asiamat.2009.2.
- [25] VICENTE, J. de; KLINGENBERG, D. J., and HIDALGO-ALVAREZ, R.: Magnetorheological fluids: a review. In: Soft Matter 7.8 (2011), p. 3701. ISSN: 1744-683X. DOI: 10.1039/c0sm01221a.
- [26] ASHTIANI, M.; HASHEMABADI, S. H., and GHAFFARI, A.: A review on the magnetorheological fluid preparation and stabilization. In: Journal of Magnetism and Magnetic Materials 374 (2015), pp. 716–730. ISSN: 03048853. DOI: 10.1016/j.jmmm.2014.09.020.
- [27] RAMLI, H.; ZAINAL, N. F. A.; HESS, M., and CHAN, C. H.: Basic principle and good practices of rheology for polymers for teachers and beginners. In: Chemistry Teacher International 4.4 (2022), pp. 307–326. DOI: 10.1515/cti-2022-0010.
- [28] PAPANASTASIOU, T. C.; GEORGIOU, G. C., and ALEXANDROU, A. N.: Viscous fluid flow. Boca Raton FL: CRC Press, 2000. ISBN: 0-8493-1606-5.
- [29] XU, X. and GUPTA, N.: Determining elastic modulus from dynamic mechanical analysis: A general model based on loss modulus data. In: Materialia 4 (2018), pp. 221–226. ISSN: 25891529. DOI: 10.1016/j.mtla.2018.09.034.
- [30] MALVERN INSTRUMENT WORLDWIDE: A Basic Introduction to Rheology: Whitepaper. 2016.
- [31] ZINCHENKO, G. A.; MILESHKEVICH, V. P., and KOZLOVA, N. V.: Investigation of the synthesis and hydrolytic degradation of polyborodimethylsiloxanes. In: Polymer Science U.S.S.R. 23.6 (1981), pp. 1421–1429. ISSN: 00323950. DOI: 10.1016/0032-3950(81)90109-X.
- [32] JONAS REUSS: Untersuchungen zu den herstellungsbezogenen und rheologischen Eigenschaften von Borosilikonkitt. Master Thesis. Ilmenau, Germany: Technische Universität Ilmenau, 2016.
- [33] WEIJERMARS, R.: Flow behaviour and physical chemistry of bouncing putties and related polymers in view of tectonic laboratory applications. In: Tectonophysics 124.3-4 (1986), pp. 325–358. ISSN: 00401951. DOI: 10.1016/0040-1951(86)90208-8.

- [34] MYRONIDIS, K.; THIELKE, M.; KOPEĆ, M.; MEO, M., and PINTO, F.: Polyborosiloxane-based, dynamic shear stiffening multilayer coating for the protection of composite laminates under Low Velocity Impact. In: *Composites Science and Technology* 222 (2022), p. 109395. ISSN: 02663538. DOI: 10.1016/j.compscitech.2022.109395.
- [35] BASF: BASF continues to evolve carbonyl iron powders. In: *Metal Powder Report* 54.3 (1999), pp. 18–20. ISSN: 00260657. DOI: 10.1016/S0026-0657(99)80339-7.
- [36] BASF THE CHEMICAL COMPANY: Carbonyl Iron Powder. 2012.
- [37] SEETAPAN, N.; FUONGFUCHAT, A.; SIRIKITTIKUL, D., and LIMPARYOON, N.: Unimodal and bimodal networks of physically crosslinked polyborodimethylsiloxane: viscoelastic and equibiaxial extension behaviors. In: *Journal of Polymer Research* 20.7 (2013). ISSN: 1022-9760. DOI: 10.1007/s10965-013-0183-8.
- [38] RAMIREZ, A. and VILCA, M.: Rheological properties of polyborosiloxane (PBS) and its application in tensegrity structure. Germany, 29.05.2023.
- [39] BLUDAU, H.: *Praktikum Borhaltige Polysiloxane: Wahlpraktikum für Bachelor Chemie*. 2013.
- [40] LAI, W.; WANG, Y., and HE, J.: Effects of Carbonyl Iron Powder (CIP) Content on the Electromagnetic Wave Absorption and Mechanical Properties of CIP/ABS Composites. In: *Polymers* 12.8 (2020). DOI: 10.3390/polym12081694.
- [41] ZHANG, G.; WANG, H.; WANG, J.; ZHENG, J., and OUYANG, Q.: The impact of CIP content on the field-dependent dynamic viscoelastic properties of MR gels. In: *Colloids and Surfaces A: Physicochemical and Engineering Aspects* 580 (2019), p. 123596. ISSN: 09277757. DOI: 10.1016/j.colsurfa.2019.123596.
- [42] THE UNIVERSITY OF UTAH: *Rheometry Basics*. Ed. by PORTER BIEHLER. <https://mcl.mse.utah.edu/basics/>, 2023.
- [43] LI, Z.; LI, D.; CHEN, Y.; YANG, Y., and YAO, J.: Influence of Viscosity and Magneto-viscous Effect on the Performance of a Magnetic Fluid Seal in a Water Environment. In: *Tribology Transactions* 61.2 (2018), pp. 367–375. ISSN: 1040-2004. DOI: 10.1080/10402004.2017.1324071.
- [44] ANTON PAAR: *Basic of Dynamic Mechanical Analysis (DMA)*. web page, 2023.
- [45] KABOORANI, A. and BLANCHET, P.: Determining the Linear Viscoelastic Region of Sugar Maple Wood by Dynamic Mechanical Analysis. In: *BioResources* 9.3 (2014). DOI: 10.15376/biores.9.3.4392-4409.
- [46] MEZGER, T. G.: *Das Rheologie Handbuch. Vincentz Network*, 2019. ISBN: 9783748600121. DOI: 10.1515/9783748600121.
- [47] ANTON PAAR: *Amplitude Sweeps*. Ed. by ANTON PAAR. 2023.

- [48] RHEOLOGY TESTING SERVICES: Frequency sweep: "Getting all shock up": Probing viscoelastic properties and molecular interactions. Ed. by RHEOLOGY TESTING SERVICES. <https://www.rheologytestingservices.com/frequency-sweep>, 2017.
- [49] WENBIN, C.; XIANG, F.; JINGMING, C., and CAIHUA, X.: Design and analysis of passive variable stiffness device based on shear stiffening gel. In: *Smart Materials and Structures* 31.12 (2022), p. 125007. ISSN: 0964-1726. DOI: 10.1088/1361-665X/ac9dd4.
- [50] ANTON PAAR: Avoid Measurement Errors in Rheometry: Shear waves in low-viscosity liquids. Ed. by ANTON PAAR. 2023.
- [51] EMBRY-RIDDLE AERONAUTICAL UNIVERSITY: Hemholtz Coils. Ed. by EMBRY-RIDDLE AERONAUTICAL UNIVERSITY. n.d.
- [52] BEIRANVAND, R.: Magnetic field uniformity of the practical tri-axial Helmholtz coils systems. In: *The Review of scientific instruments* 85.5 (2014), p. 055115. DOI: 10.1063/1.4876480.
- [53] PERKIN ELMER: A beginner's guide: Thermogravimetric analysis (TGA). Ed. by PERKIN ELMER. 2015.
- [54] AMERICAN SOCIETY FOR TESTING AND MATERIALS: Standard Test Method for Compositional Analysis by Thermogravimetry. 2020.
- [55] ROYAL SOCIETY OF CHEMISTRY: Silicon. Royal Society of Chemistry, 2023.
- [56] MIANDAD, R.; REHAN, M.; BARAKAT, M. A.; ABURIAZAIZA, A. S.; KHAN, H.; ISMAIL, I. M. I.; DHAVAMANI, J.; GARDY, J.; HASSANPOUR, A., and NIZAMI, A.-S.: Catalytic Pyrolysis of Plastic Waste: Moving Toward Pyrolysis Based Biorefineries. In: *Frontiers in Energy Research* 7 (2019). DOI: 10.3389/fenrg.2019.00027.
- [57] RAN, G.; LIU, X.; GUO, J.; SUN, J.; LI, H.; GU, X., and ZHANG, S.: Improving the flame retardancy and water resistance of polylactic acid by introducing polyborosiloxane microencapsulated ammonium polyphosphate. In: *Composites Part B: Engineering* 173 (2019), p. 106772. ISSN: 13598368. DOI: 10.1016/j.compositesb.2019.04.033.
- [58] SIGMA-ALDRICH: What is FTIR Spectroscopy? Ed. by SIGMA-ALDRICH. 2023.
- [59] THERMO FISHER SCIENTIFIC: FTIR Spectroscopy Academy: Thermo Scientific FTIR spectrometer and microscope resources. Ed. by THERMO FISHER SCIENTIFIC. 2023.
- [60] LI, X.; ZHANG, D.; XIANG, K., and HUANG, G.: Synthesis of polyborosiloxane and its reversible physical crosslinks. In: *RSC Adv* 4.62 (2014), pp. 32894–32901. DOI: 10.1039/c4ra01877j.
- [61] CHRUSCIEL, J.; FEJDYŚ, M., and FORTUNIAK, W.: Synthesis and characterization of new, liquid, branched poly(methylvinylborosiloxanes). In: *e-Polymers* 13.1 (2013). ISSN: 2197-4586. DOI: 10.1515/epoly-2013-0134.

-
- [62] PURDUE UNIVERSITY: Scanning Electron Microscope. Ed. by PURDUE UNIVERSITY. 2019.
- [63] WU, Y.; CHEN, L.; HAN, Y.; LIU, P.; XU, H.; YU, G.; WANG, Y.; WEN, T.; JU, W., and GU, J.: Hierarchical construction of CNT networks in aramid papers for high-efficiency microwave absorption. In: *Nano Research* 16.5 (2023), pp. 7801–7809. ISSN: 1998-0124. DOI: 10.1007/s12274-023-5522-4.
- [64] APPIAH, C.; ARNDT, C.; SIEMSEN, K.; HEITMANN, A.; STAUBITZ, A., and SELHUBER-UNKEL, C.: Living Materials Herald a New Era in Soft Robotics. In: *Advanced materials* (Deerfield Beach, Fla.) 31.36 (2019), e1807747. DOI: 10.1002/adma.201807747.
- [65] HAINES, C. S.; LI, N.; SPINKS, G. M.; ALIEV, A. E.; DI, J., and BAUGHMAN, R. H.: New twist on artificial muscles. In: *Proceedings of the National Academy of Sciences of the United States of America* 113.42 (2016), pp. 11709–11716. DOI: 10.1073/pnas.1605273113.



Used abbreviations

| | |
|-------------|---|
| PBS | polyborosiloxane |
| CIP | carbonyl-iron-powder |
| MRF | magnetorheological fluid |
| LVER | linear viscoelastic region |
| PDMS | polydimethylsiloxane |
| BA | boric-acid |
| SSG | shear stiffening gel |
| DMA | dynamic mechanical analysis |
| MF | magnetic field |
| ABS | acrylonitrile butadiene styrene |
| CPE | chlorinated polyethylene |
| VSM | vibrating sample magnetometer |
| TGA | thermogravimetric analysis |
| FTIR | Fourier transform infrared spectroscopy |
| SEM | scanning electron microscope |
| ATR | attenuated total reflectance |
| OSHA | Occupational Safety and Health Administration |
| PUCP | Pontificia Universidad Católica del Perú |
| PS | polystyrene |
| PP | polypropylene |
| PET | polyethylene terephthalate |
| PE | polyethylene |
| APP | ammonium polyphosphate |

List of Figures

| | | |
|------|--|----|
| 1.1 | Molecular structure of main precursors of PBS: (a) Boric acid; (b) Polydimethylsiloxane | 2 |
| 2.1 | Examples of the different categories of smart materials: (a) Passive smart material (optical fiber); (b) Active smart material (piezoelectric material) [21, 24] | 5 |
| 2.2 | Behavior of MRF: (a) Under normal conditions; (b) Under the effect of a magnetic field [21] | 6 |
| 2.3 | Two plate model[27] | 7 |
| 2.4 | Summary of different types of fluids: (a) Shear stress as function of shear rate; (b) Viscosity as function of shear rate. [27] | 9 |
| 2.5 | Complex dynamic modulus adapted from [30] | 9 |
| 2.6 | Example of storage and loss modulus, extracted from [27] | 10 |
| 2.7 | Burgers or four element model and its shear strain response through time [27] | 12 |
| 2.8 | PBS possible molecular structures, proposed by Zinchenko et al. [6, 8, 31] | 13 |
| 2.9 | Temporary cross-linking bonds between chains, adapted from [33] | 14 |
| 2.10 | PBS speed dependent behavior, extracted from [34] | 14 |
| 4.1 | Complete set up for the synthesis of PBS: 1.Universal magnetic stand; 2.Temperature display; 3.Thermometer; 4.Tall beaker (mix go inside); 5.Low beaker (Oil go inside); 6.Hotplate magnetic stirrer | 20 |
| 4.2 | Oven Binder Model FD 23 with timer function and air exhaust | 21 |
| 4.3 | Laboratory fume cupboard Brand Waldner model secuflow: 1.Quick access windows; 2.Inner Plug; 3.Complete set up | 21 |
| 4.4 | VSM results of CIP ratios of CIP:CPE a.12:1; b.14:1; c.16:1, extracted from [8] | 23 |
| 4.5 | Mixing process of PBS and CIP | 24 |
| 4.6 | Two types of geometries within rotational rheometers: (a) Plate-plate geometry; (b) Cone-plate geometry, adapted from [30] | 25 |
| 4.7 | Input and output measures of a rheometer representing the behavior of a elastic, viscoelastic and viscous material, extracted from [30] | 26 |
| 4.8 | Rheometer Malvern-Netzsch model Kinexus Pro + | 26 |
| 4.9 | Plate-plate geometry used for amplitude and frequency sweep tests: (a) Upper geometry ($\phi 25$ mm); (b) Lower geometry ($\phi 25$ mm) | 27 |
| 4.10 | Storage modulus results of amplitude sweep of different amounts of PBS mixed with CIP | 28 |
| 4.11 | Loss modulus results of amplitude sweep of different amounts of PBS mixed with CIP | 29 |

List of Figures

| | | |
|------|--|-------|
| 4.12 | Evidence of the surpass of the LVER: before and after the amplitude sweep test respectively | 29 |
| 4.13 | Frequency sweep results of different amounts of PBS mixed with CIP | 31 |
| 4.14 | Frequency sweep results SSG reinforced with CaCO ₃ particles, extracted from [19] | 32 |
| 4.15 | Frequency sweep results SSG, extracted from [49] | 33 |
| 4.16 | Shape change test configuration: 1.Camera; 2.Camera tripod; 3.Helmholtz coil | 34 |
| 4.17 | Magnetic field distribution of a Helmholtz coil, extracted from [51] | 35 |
| 4.18 | Measure of the pulsating magnetic field for 1 Hz | 36 |
| 4.19 | Diameter increase percentage over time | 37 |
| 4.20 | PBS TGA results | 39 |
| 4.21 | PS, PE, PP, and PET TGA results from [56] | 40 |
| 4.22 | PBS-20 TGA results | 41 |
| 4.23 | PBS-80 TGA results | 42 |
| 4.24 | FTIR results of PBS, PBS-20 and PBS-80 | 43 |
| 4.25 | SEM images of pure PBS: 500; 1000; 2500; 5000 magnifications | 44 |
| 4.26 | SEM images of PBS-20: 500; 1000; 2000; 5000; 10000 magnifications | 45 |
| 4.27 | SEM images of PBS-40: 500; 1000; 2000; 5000; 10000 magnifications | 46 |
| 4.28 | SEM images of PBS-60: 500; 1000; 2000; 5000; 10000 magnifications | 46 |
| 4.29 | SEM images of PBS-80: 500; 1000; 2000; 5000; 10000 magnifications | 47 |
| | | |
| A.1 | Amplitude sweep results of five samples of PBS | XXI |
| A.2 | Amplitude sweep results of five samples of PBS-20 | XXI |
| A.3 | Amplitude sweep results of five samples of PBS-40 | XXII |
| A.4 | Amplitude sweep results of five samples of PBS-60 | XXII |
| A.5 | Amplitude sweep results of five samples of PBS-80 | XXIII |
| A.6 | Frequency sweep results of five samples of PBS | XXIV |
| A.7 | Frequency sweep results of five samples of PBS-20 | XXIV |
| A.8 | Frequency sweep results of five samples of PBS-40 | XXV |
| A.9 | Frequency sweep results of five samples of PBS-60 | XXV |
| A.10 | Frequency sweep results of five samples of PBS-80 | XXVI |

List of Tables

| | | |
|-----|---|----|
| 2.1 | Chemical composition and average diameter of CIP type CC [36] | 15 |
| 4.1 | Composition of prepared samples | 23 |
| 4.2 | Viscoelastic parameters possible to measure through DMA | 26 |
| 4.3 | Parameters of the amplitude sweep test | 28 |
| 4.4 | Average limit of the LVER of all the samples | 30 |
| 4.5 | Parameters of the frequency sweep test | 30 |
| 4.6 | Average gel points of all the samples | 33 |
| 4.7 | Shape change results | 36 |
| 4.8 | TGA parameters followed by ASTM E1131 [54] | 38 |
| A.1 | Mass losses due synthesis of PBS | XX |

List of formula symbols

| Formula symbol | Definition | Unit |
|----------------|--------------------------|---------------|
| F | Force | N |
| A | Area | m^2 |
| σ | Shear stress | Pa |
| η | Dynamic viscosity | Pa s |
| γ | shear strain | $\frac{m}{m}$ |
| Δx | Displacement | m |
| $\dot{\gamma}$ | Shear rate | $\frac{1}{s}$ |
| δ | Phase angle | $^\circ$ |
| ν | Poisson Ratio | $\frac{m}{m}$ |
| E | Elastic module | MPa |
| ϵ | Tensile strain | $\frac{m}{m}$ |
| G | Shear module | MPa |
| G' | storage modulus | Pa |
| G'' | Loss modulus | Pa |
| G^* | Complex modulus | Pa |
| τ | Relaxation time | s |
| H | Magnetic field | T |
| σ_s | Saturation magnetization | emu/g |
| Hc | Coercivity | Oe |

A. Appendix

Here are the annexes with complementary information of some topics covered in the research.

A.1. Appendix 1

Here are presented a table with mass loss product of the synthesis of PBS made with a PDMS with a viscosity of 750 cSt.

Table A.1.: Mass losses due synthesis of PBS

| Sample pure PBS | | |
|-----------------|----------------------|-------------------|
| Item | Theoretical mass (g) | Measured mass (g) |
| PDMS2 | 40.000 | 40.008 |
| BA | 1.2 | 1.202 |
| Final mass | 41.200 | 36.847 |
| Mass loss | 0% | 10.6% |

A.2. Appendix 2

Here are the graphics of every 5 results per all the kinds of samples measured for the amplitude sweep test.

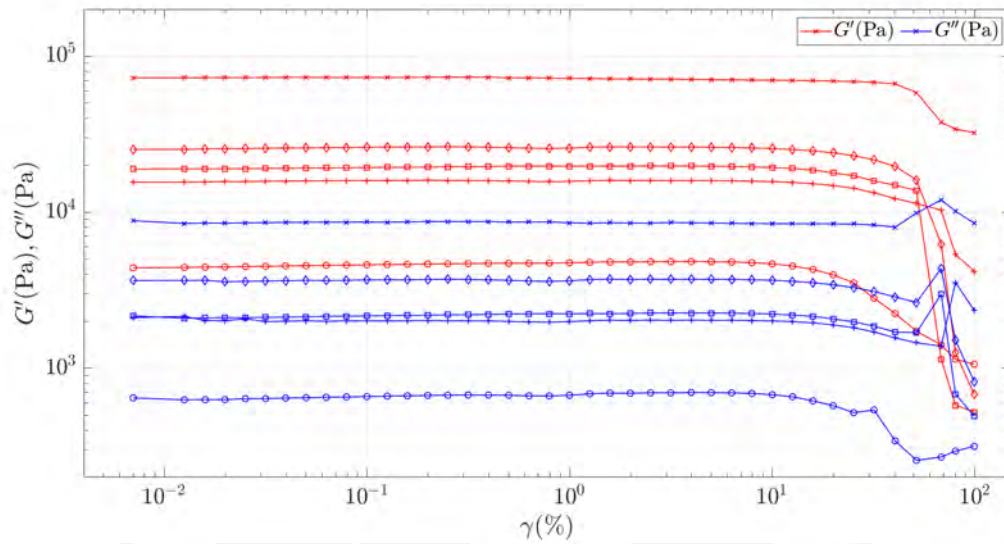


Figure A.1.: Amplitude sweep results of five samples of PBS

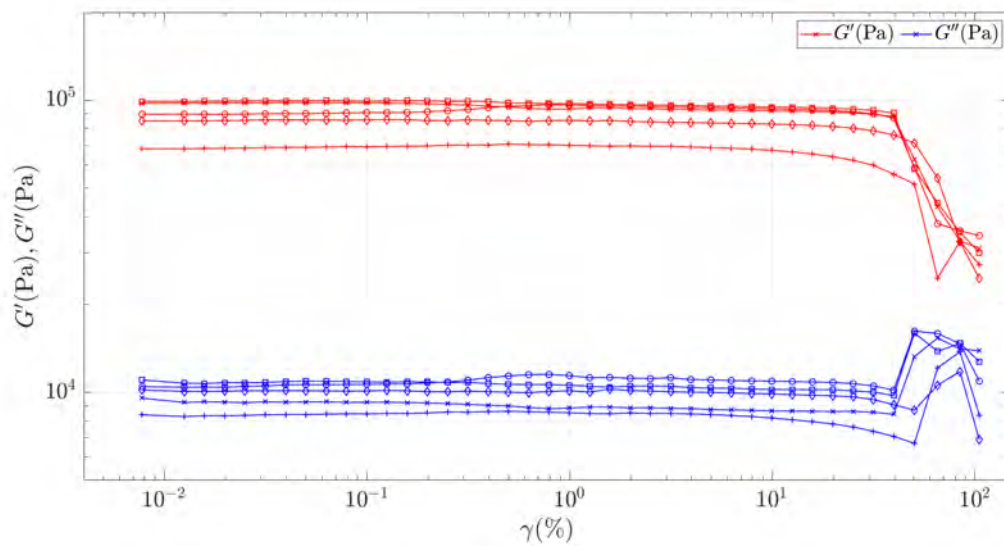


Figure A.2.: Amplitude sweep results of five samples of PBS-20

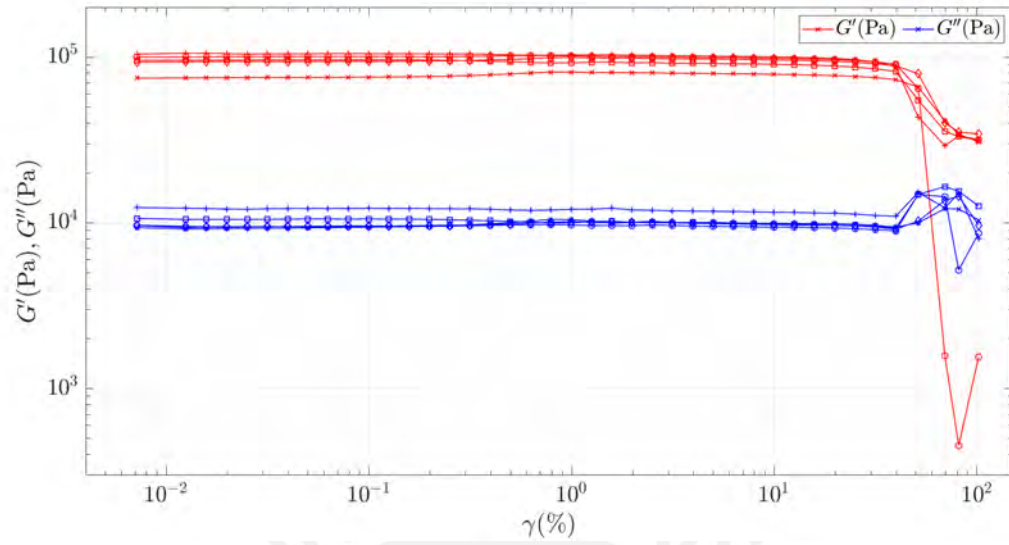


Figure A.3.: Amplitude sweep results of five samples of PBS-40

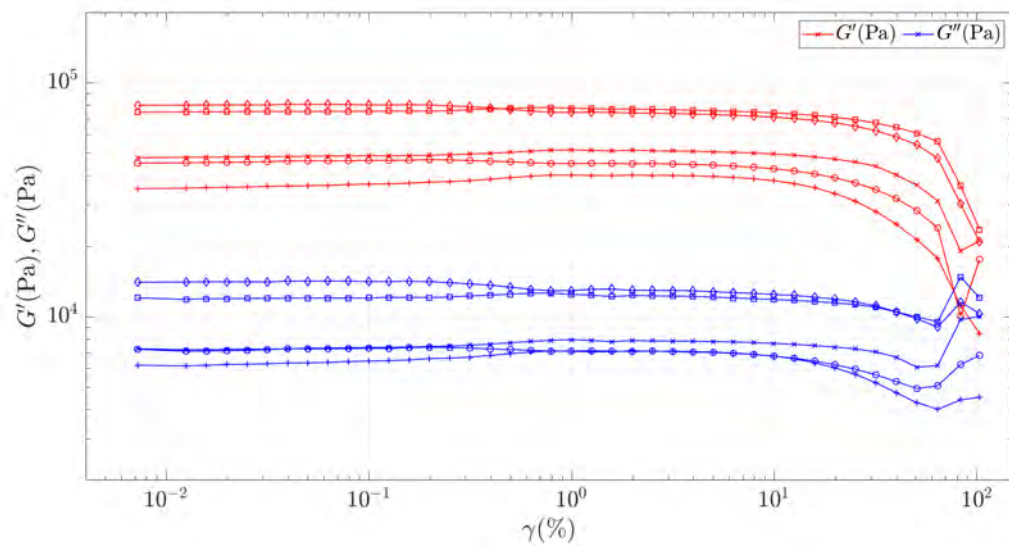


Figure A.4.: Amplitude sweep results of five samples of PBS-60

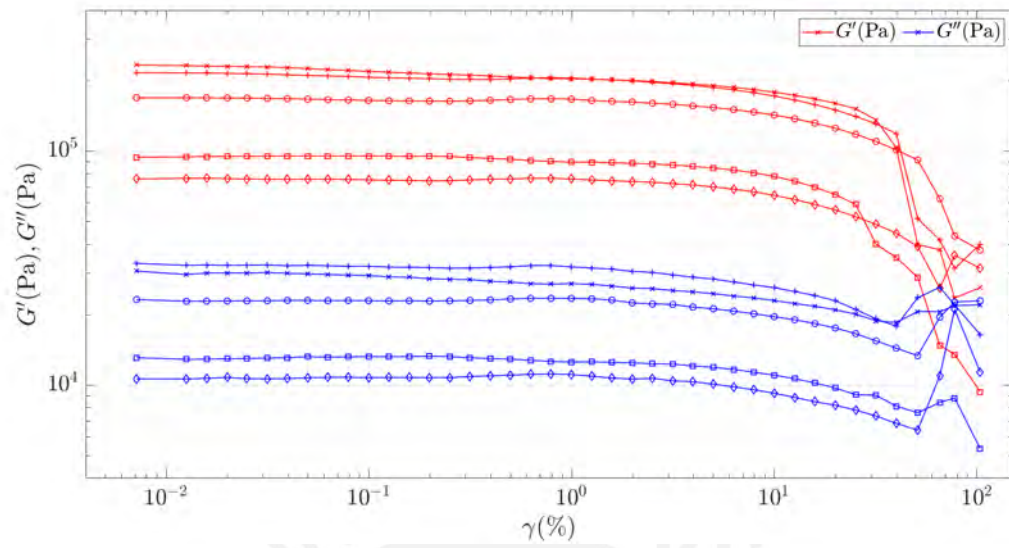
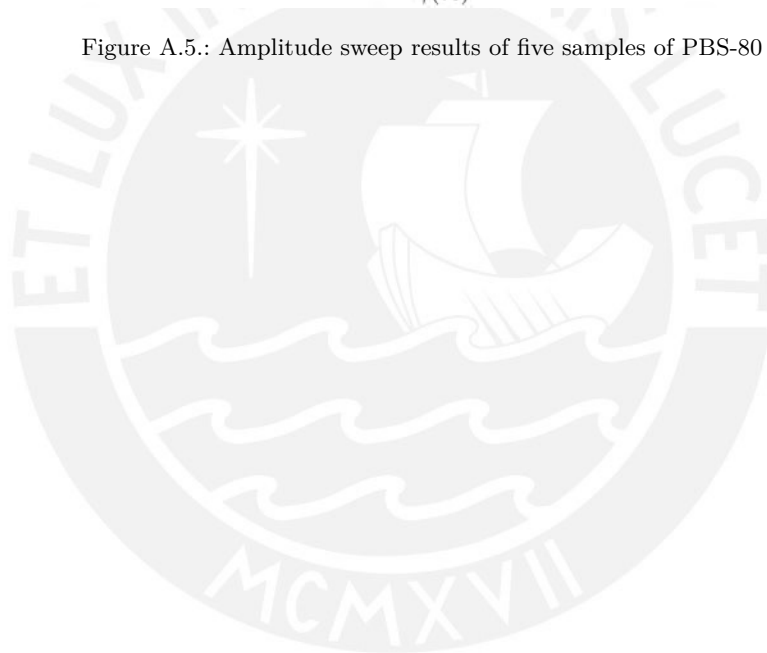


Figure A.5.: Amplitude sweep results of five samples of PBS-80



A.3. Appendix 3

Here are the graphics of every 5 results per all the kinds of samples measured for the frequency sweep test.

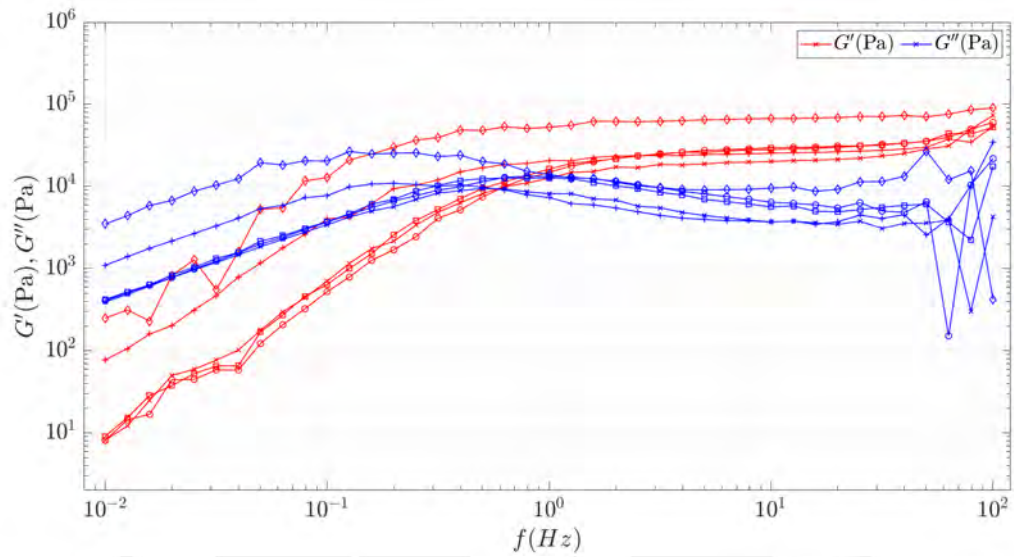


Figure A.6.: Frequency sweep results of five samples of PBS

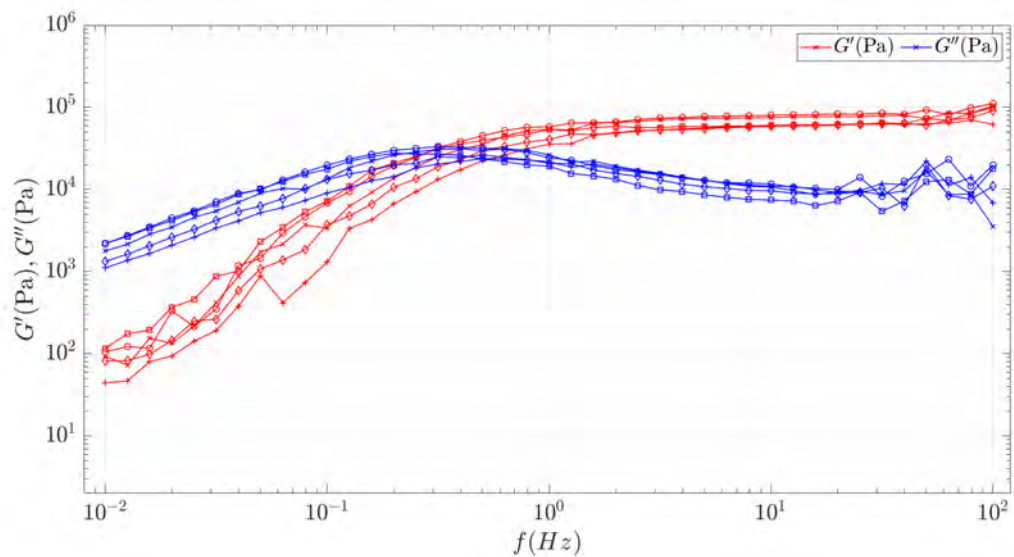


Figure A.7.: Frequency sweep results of five samples of PBS-20

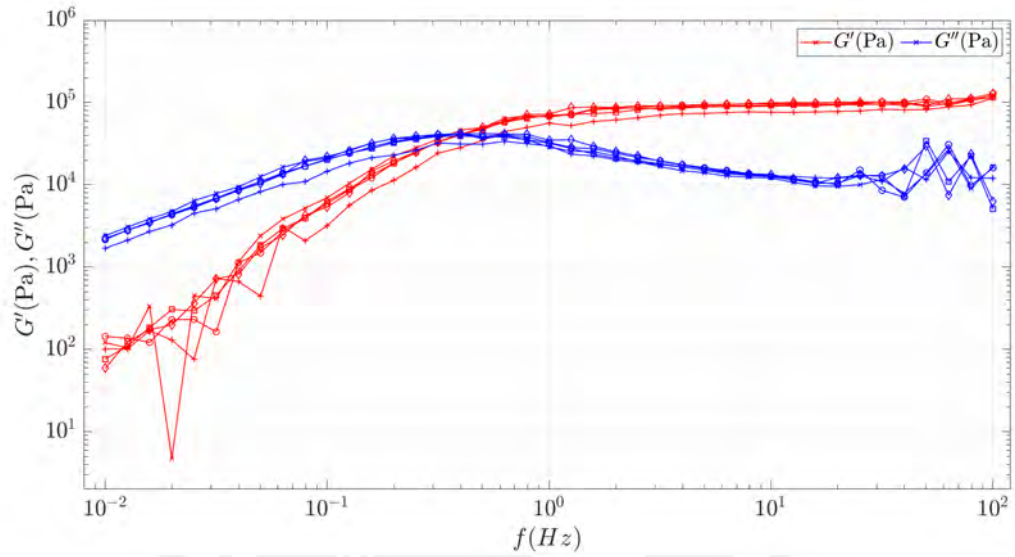


Figure A.8.: Frequency sweep results of five samples of PBS-40

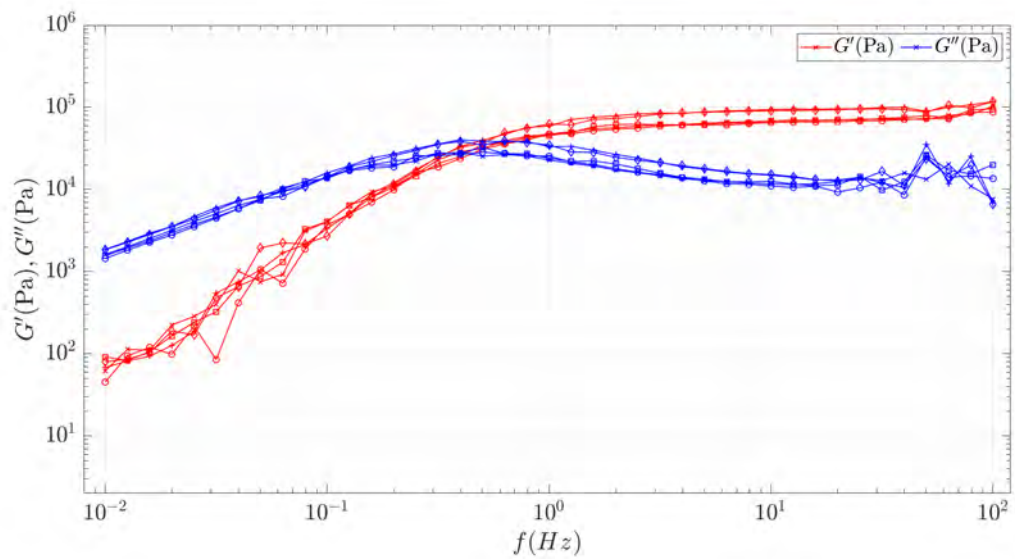


Figure A.9.: Frequency sweep results of five samples of PBS-60

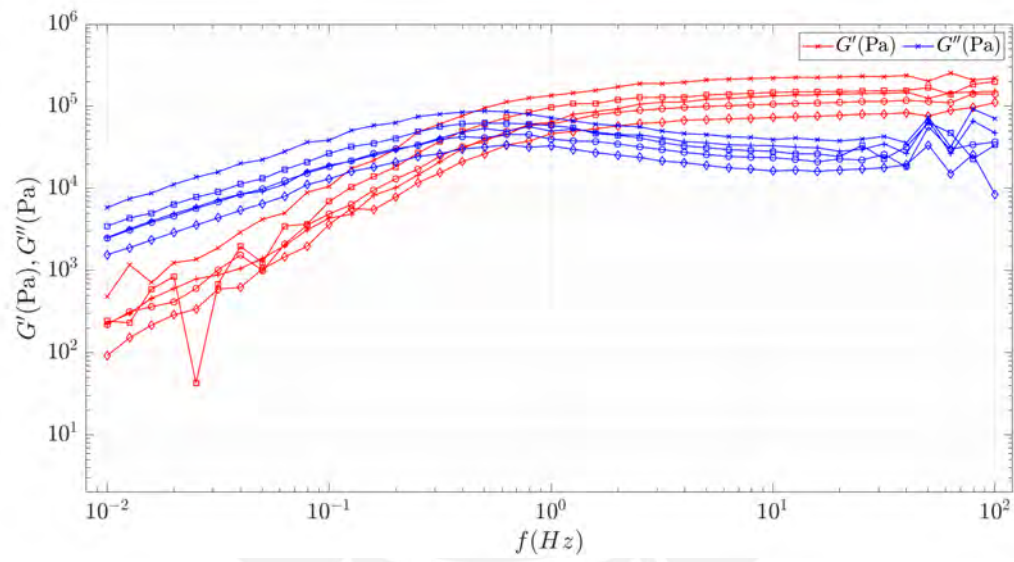


Figure A.10.: Frequency sweep results of five samples of PBS-80

Statement

I hereby declare that I have completed this work independently and without using any tools other than those specified. The ideas taken literally or analogously from other people's works are marked and the sources are indicated. I certify that I have not yet submitted any examination paper with the same or similar topic to an examination authority or other university.

Ilmenau, 14.12.2023

Miguel Alberto Vilca Bendezú

